RHEOLOGY OF CRYSTALLIZING BASALTS FROM NYIRAGONGO AND NYAMURAGIRA VOLCANOES, D.R.C.

A Thesis

presented to

the Faculty of the Graduate School

at the University of Missouri-Columbia

In Partial Fulfillment

of the Requirements for the Degree

Master of Science

---

by

AARON MORRISON

Dr. Alan Whittington, Thesis Supervisor

MAY 2016

The undersigned, appointed by the dean of the Graduate School, have examined the thesis entitled

RHEOLOGY OF CRYSTALLIZING BASALTS FROM
NYIRAGONGO AND NYAMURAGIRA VOLCANOES, D.R.C.

presented by Aaron Morrison,

a candidate for the degree of master of science,

and hereby certify that, in their opinion, it is worthy of acceptance.

Professor Alan Whittington

Professor Michael Underwood

Professor Stephen Lombardo

ACKNOWLEDGEMENTS

This work was supported by NSF EAR-1220051 and NASA PPG-NNX12AO44G awarded to Dr. Alan Whittington. I would like to thank Paul Carpenter (Washington University in St. Louis) and Jim Schiffbauer (University of Missouri) for assistance and instruction in EPMA and SEM techniques. I would also like to thank Matthieu Kervyn, Benoit Smets, and Sam Poppe from Vrije Universiteit Brussel, Belgium, for sample collection and meaningful discussion of pertinent details. Finally, I must thank Dr. Alan Whittington and Dr. Alex Sehlke for the guidance, tutelage, and facilitation of this research project.

TABLE OF CONTENTS

LIST OF FIGURES

LIST OF TABLES

RHEOLOGY OF CRYSTALLIZING BASALTS FROM NYIRAGONGO AND NYAMURAGIRA VOLCANOES, D.R.C.

Abstract

Nyiragongo, a stratovolcano located within the Virunga Volcanic Province on the western branch of the East African Rift, is known for its persistent lava lake activity as well as devastating eruptions in 1977 and 2002. The 2002 eruption caused a humanitarian crisis when channelized lava flows entered the nearby city of Goma killing 170 people and displacing ~350,000 others. These lavas have unusually low silica contents (39-42 wt.% SiO_2) and are very fluid, allowing flows to move rapidly down the volcano's flanks. The rheology of lavas from Nyiragongo was measured using a concentric cylinder viscometer over a range of temperatures between 1221°C and 1145°C. The viscosity is ~33 Pa s at the liquidus temperature of ~1213°C, similar to Hawaiian lavas (30 Pa s near their liquidus temperature of ~1230°C), increasing gradually to ~708 Pa s at 1145˚C. Over this temperature range, the crystal fraction remains very low ($\varphi_c \leq 0.02$) until ~50°C undercooled and is still only ~0.05 at 1145˚C, where the viscosity of the starting bulk melt would be ~123 Pa s and that of the interstitial melt is ~1323 Pa s. Consequently, the change in viscosity is due primarily to cooling effects rather than the physical or chemical effects of crystallization. The data were collected at strain rates between ~0.4 and 46.3s^{-1}, and are well reproduced using a power-law model with exponents decreasing from 0.96 (1221°C) to ~0.78 (1145°C) and no detectable yield strength. Crystal fraction and lava viscosity both increase rapidly below 1145˚C, preventing further experiments.

Lavas from the neighboring shield volcano, Nyamuragira, show significant crystallization at temperatures much closer to the liquidus and so pseudo-plastic behavior is observed much closer to the liquidus as well. Data are again well reproduced by a power-law fit with flow indices ranging from between 0.89 (1255°C) and ~0.42 (1154°C). While still fairly fluid, having a liquid viscosity of ~46 Pa s, it is more viscous than Nyiragongo lavas and also crystallizes more rapidly upon undercooling, reaching an effective viscosity of ~1110 Pa s at 1154˚C.

In recent years, the steep-sided stratovolcano Nyiragongo has erupted lava that is more fluid than erupted by the nearby shield volcano, Nyamuragira, producing fast-moving flows that pose imminent danger to the inhabitants of Goma. Consequently, lava flow inundation hazard cannot be predicted solely by the morphology of the volcanoes from which the flows erupt.

Introduction

Lava flows are usually regarded as relatively modest volcanic hazards when compared to the faster and farther reaching hazards (i.e. pyroclastic density currents, lahars, or debris flows). Yet, hot, fluid, mafic lavas are capable of advancing rapidly and are particularly hazardous when human settlements encroach on steep volcanic flanks. While the Hawaiian volcanoes (Kilauea and Mauna Loa) may be the first to come to mind, other pertinent examples of this would be Nyiragongo and Nyamuragira volcanoes: the two most active volcanoes in the Virunga Volcanic Province (VVP) of east-central Africa (Figure 1).

The East African Rift System (EARS) runs for over 2000 km through the eastern African continent from the Red Sea to Mozambique (Chakrabarti et al., 2009a). East African Rift volcanism spans the entire range from felsic to ultramafic compositions (Andersen et al., 2012). The northern region is typified by voluminous flood basalt eruptions approximately 30 Mya related to the Afar mantle plume (Schilling et al., 1992; Chakrabarti et al., 2009a). Further south, the rift system breaks into an eastern branch running through Ethiopia, Kenya, and parts of Tanzania, and a western branch running through Rwanda, the Democratic Republic of Congo and parts of Uganda. The EARS has been suggested to divide into these two branches around a microplate centered on the Tanzanian Craton (Calais et al., 2006; Saria et al., 2014). Within the western branch of this division lies the VVP, located mainly in the Democratic Republic of the Congo (D.R.C.) near the border of Uganda and Rwanda. This province contains eight volcanoes only two of which are active (Demant et al., 1994): Nyamuragira (commonly: Nyamulagira) and Nyiragongo, with the former being the most active volcano in Africa

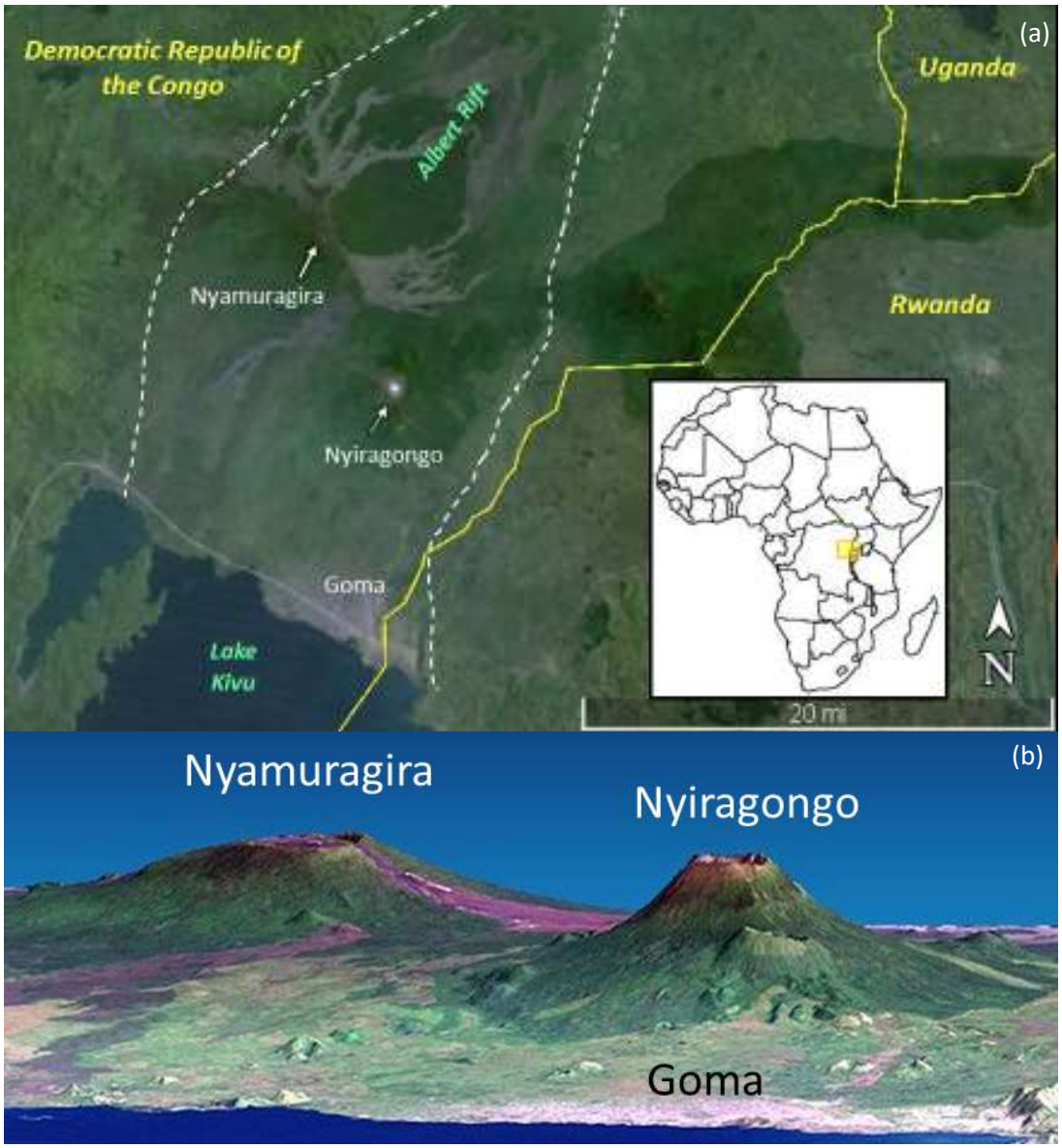

Figure 1: *(a) Nyiragongo and Nyamuragira volcanoes located in the western Virunga Volcanic Province. These volcanoes lie in the active, NNE-SSW trending Albert Rift which is a part of the western branch of the EARS. The city of Goma lies just on the southern flank of Nyiragongo. (b) Topographic model showing different volcano morphologies of Nyiragongo and Nyamuragira based on data from Landsat and Shuttle Radar Topography Mission. Vertical exaggeration of 1.5x, credit to NASA/JPL/NIMA. Further information: Photo ID: PIA03337, Public Domain, https://commons.wikimedia.org/w/index.php?curid=3253747*

(Coppola and Cigolini, 2013) and the latter erupting some of the lowest viscosity silicate lavas on Earth (Giordano et al., 2007; Chakrabarti et al., 2009a; Chakrabarti et al., 2009b). While these two volcanoes are separated by only 15 km, they produce very different lavas suggesting the volcanoes sample different sources or have different degrees of differentiation (Chakrabarti et al., 2009a; Andersen et al., 2012).

Nyiragongo

Nyiragongo is a stratovolcano (Figure 1) rising approximately 3470 m above sea level, located 15 km north of Lake Kivu in eastern D.R.C. near the border of Uganda and Rwanda. This volcano has been widely known for its persistent lava lake activity as well as its unique composition (Platz et al., 2004; Tedesco et al., 2007; Andersen et al., 2012). The main crater is roughly 1.3 km in diameter with a lava lake approximately 200 m across making it the largest persistent lava lake in the world (Sawyer et al., 2008). Nyiragongo lavas are mafic, foiditic (39.61 wt% SiO_2), ultra-alkaline (5.47 wt% Na_2O; 5.14 wt% K_2O) lavas (Chakrabarti et al., 2009a, 2009b) which form extremely low viscosity flows (Figure 2). Giordano et al. (2007) report thermal and rheological properties for 2002 Nyiragongo lavas. Flow speeds (from eye witness accounts) and thermal diffusivities were assumed; viscosities and flow thicknesses were measured; and eruptive temperatures were calculated. Their experiments suggest these lavas have the lowest viscosity of any terrestrial silicate lava, with only carbonatite lavas being more fluid (Dawson et al., 1990). The volcanic system itself is composed of the main cone of Nyiragongo as well as several extinct cones to the north (Baruta) and south (Shaheru) (Andersen et al., 2012).

There have been only two recorded eruptions (activity occurring outside the caldera) since Nyiragongo was first described in 1896 (Von Gotzen, 1896). During the 1977 eruption, the city of Goma had a population of around 50,000 (Tedesco et al., 2007). Subsequently, the city expanded northward toward the volcano growing into a city of over 500,000 people due to the influx of refugees from neighboring Rwanda and the civil unrest wracking nearby countries. This set the stage for the eruption in January of 2002 to be one of the most devastating eruptions to human life in recent history. A very thorough chronology of the 2002 eruption is compiled in Tedesco et al. (2007).

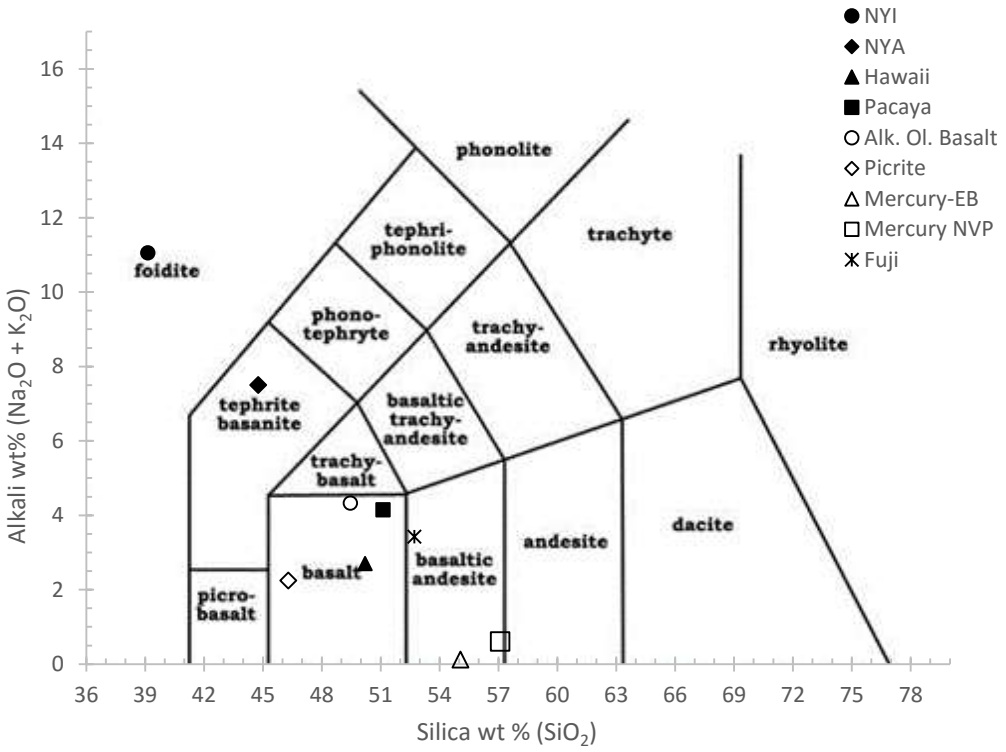

Figure 2. *TAS diagram plotting compositions of this study (NYI and NYA) in relation to other key basaltic compositions [Hawaii: Sehlke et al., (2014); Mercury-Enstatite Basalt (EB) and Northern Volcanic Plains (NVP): Sehlke et al., (2015); Pacaya: Soldati et al., (2015); Picrite: Ryerson et al., (1988); Fuji: Ishibashi and Sato (2010); Ishibashi and Sato (2007)].*

On the southern flank of Nyiragongo (Shaheru region), activity is driven mainly by drainage of the partially solidified, degassed, lava lake and conduit inside the main Nyiragongo crater. While some studies disagree about the early historical activity (Tazieff, 1984; Demant et al., 1994; Simkin and Siebert, 1994), most of the literature does agree that persistent lava lake activity occurred from 1928 until the 1977 eruption that drained the caldera. Lava lakes returned in 1982 and 1994 before civil unrest in the region made observation impractical. A roughly north-south oriented fracture system (Munigi Fissure) propagates from the main summit crater through the city of Goma and into Lake Kivu. This system developed during the 1977 eruption and further propagated in 2002 facilitating the erupted lava's infiltration into the city (Tazieff, 1977; Carn, 2002; Sawyer et al., 2008). Lavas erupted from this fracture system are gas-rich, driving fountaining processes, in contrast to the relatively degassed lava lake in the main crater.

Nyiragongo garnered international attention during its 2002 eruption. The city of Goma rests on the edge of Lake Kivu and the southern flank of the volcano with a population of around 500,000 (Tedesco et al., 2007). During this eruption, the extremely low viscosity lavas rapidly infiltrated the town killing 170 people and displacing nearly 350,000 others. A major contributing factor to this humanitarian crisis was the formation of a fracture system that propagated into the city allowing for the rapid infiltration of the already fast flowing lava (Carn, 2002; Acocella and Neri, 2009). Potential hazards increased due to the influx of Rwandan refugees to the area as well as SO_2 emissions occurring in downtown Goma (Carn, 2002; Tedesco et al., 2007). This development coupled with a lack of adequate warning or preparation proved devastating to its inhabitants. Due to the geopolitical climate in the region, few scientific studies had been

accomplished by the time of the eruption. The conflicts led to vandalization of several seismometers monitoring Nyiragongo leaving only two in working order to forecast an event (Tedesco et al., 2007; Wafula et al., n.d.; Smets et al., 2014).

Nyamuragira

Nyamuragira is a shield volcano (Figure 1) approximately 3058 m above sea level, 25 km north of Lake Kivu in eastern D.R.C. and only 15 km northwest of Nyiragongo. This volcano has been erupting approximately once every two years, with 38 major eruptions since the 1900s (Coppola and Cigolini, 2013), making it the currently, most active African volcano. Generally, lavas from Nyamuragira are alkali basalts, hawaiites, basanites and tephrites (Figure 2) with a range of silica content from 43-56 wt.% (Aoki et al., 1985). These lavas are also characteristically high in sulfur content. Remote sensing studies of SO_2 emissions indicate a strong excess of sulfur from effusive activity (Carn and Bluth 2003; Bluth and Carn 2008; Head et al., 2011), which contradicts many petrologic models that project significantly smaller S contents than observed (Wallace, 2001; Sharma et al., 2004; Shinohara, 2008). Maximum sulfur contents found in primitive melts are about 3700 ppm whereas those of evolved Nyamuragira melts would require nearly 5000 ppm to reconcile with the amount of erupted lavas (Head et al., 2011; Coppola and Cigolini, 2013). This requires pre-eruptive degassing and storage of a sulfur-rich gas phase to account for the excess sulfur concentrations observed by satellites (Sharma et al., 2004; Head et al., 2011). The mechanism driving this degassing is not well constrained due to the lack of field work achievable in the political climate of the region.

While Nyamuragira is one of the most active volcanoes in the world, civil unrest in the region has prevented the study of many eruptions between 1990 and 2010 (Wadge and Burt, 2011). Extent and duration of activity has mainly been determined by remote sensing and GVO (Goma Volcanological Observatory) reports in the Bulletin of the Global Volcanism Network. From 2010 onward, various satellites with more sophisticated imaging and detection equipment, including spectrometers, have been used to study the extent and duration of eruptive activity and volatile emissions.

During the alternating episodes of Nyiragongo's lava lake activity and quiescence, Nyamuragira has been erupting fairly regularly every 1-3 years with activity in: 1991-1993, 1994, 1996, 1998, 2000, 2001, 2002, 2004, 2006-7, 2010, 2011-12, 2014 (Wadge and Burt, 2011; Coppola and Cigolini, 2013; Smets et al., 2015). Most eruptions at Nyamuragira are lateral flank eruptions that have a very abrupt and vigorous starting point that can be very well constrained temporally. However, activity at the end of an eruption diminishes gradually making an end date much more difficult to constrain. These regular eruptions are proposed to be fed by a shallow, pressurized magma chamber which sources magmas from depth (Burt et al., 1994). A later study by Wadge and Burt (2011) characterized two main types of eruptions: short-duration events ($\leq$ 80 days) that source a shallow reservoir and long-duration events ($\geq$ 80 days) fed by a deeper source (Wauthier et al., 2013). Lava lake activity is recorded from 1929 until draining in a 1938 eruption that collapsed the caldera (Pouclet, 1976; Smets et al., 2015). Campion (2014) interpreted lava fountaining occurring in the caldera as lava lake activity but field work indicated that lava effusion rates were not high enough to maintain a molten lava basin (Smets et al., 2015).

This study attempts to quantify experimentally the rheological behavior of lavas from Nyiragongo and Nyamuragira, two volcanoes that pose a threat to the nearby city of Goma, D.R.C. Experiments were run at ambient atmospheric pressure with dry, volatile free compositions. The cooling paths and mineral assemblages of these lavas are used to determine what effect they have on viscosity and yield strength. The results show that Nyiragongo remains much more fluid over a much wider temperature range compared to nearby Nyamuragira. Compared to other basaltic compositions (Hawaii: Sehlke et al., 2014; Pacaya: Soldati et al., 2015; Mercury: Sehlke et al., 2015; Picrite: Ryerson et al., 1998), Nyiragongo displays much lower crystal fractions until ~50°C below the liquidus, resulting in lower viscosities and no detectable yield strength, which may facilitate fast moving lava flows. These results will contribute to the understanding of lava flow rheology and provide parameters for use in future hazard models for the city of Goma.

Samples

Samples from the 2002 and 1977 eruptions of Nyiragongo (1.645°S, 29.245°E; 1.63576°S, 29.248°E respectively) and the 1948 eruption of Nyamuragira (1.6126°S, 29.1262°E) were collected in 2007 by Matthieu Kervyn, Benoit Smets, and Sam Poppe from Vrije Universiteit Brussel, Belgium. Both samples from Nyiragongo were taken from just north of the city of Goma approximately 10 km south of the Shaheru vent (2 km west of the Rwandan border). The Nyamuragira samples were taken approximately 20 km from the main vent near the edge of Lake Kivu, west of Goma. The bulk composition was then analyzed by electron probe micro-analyzer (EPMA) with results summarized in Table 1. Nyiragongo lavas plot as foidites (Figure 2) as they are very silica poor (39-42 wt%), and have a high alkali content (6-12 total wt%). The Nyamuragira sample plots as a tephrite (Figure 2) with low silica (41-44 wt%) and moderate alkali content (4-9 total wt%). Both lava samples contain high amounts of iron (10-13 wt%). Thin sections of each sample were made for petrographic study (Figure 3).

The 2002 Nyiragongo sample (labeled NYI-001) shows a porphyritic texture consisting of fairly euhedral plagioclase laths (~45%) in a matrix composed of dominantly plagioclase, nepheline and pyroxene microlites (~45%). This sample is fully crystallized with no glass observed. Vesicularity in this sample is ~10% as this lava flow was degassed significantly prior to eruption. Density of the remelted glass sample was calculated to be ~2883 ± 5 kg/m^3.

The 1977 Nyiragongo sample (labeled NYI-002) shows a finer-grained texture with fewer, smaller phenocrysts (~10%). The groundmass mostly consists of plagioclase

Table 1. *Composition (in wt.%), iron oxidation, polymerization, density and liquid viscosity summaries. NYI-001 is the lava sample from the 2002 flow and NYI-002 is from the 1977 flow. NYI-002 was substituted for NYI-001 when sample material was exhausted.*

	NYI-001		NYI-002		NYA-001	
	wt%	(2σ)	wt%	(2σ)	wt%	(2σ)
SiO_2	39.13	0.43	39.61	0.48	44.76	0.51
TiO_2	2.81	0.08	2.89	0.07	3.73	0.08
Al_2O_3	14.90	0.06	14.89	0.06	16.60	0.09
FeO	12.13	0.07	12.63	0.06	11.62	0.10
MnO	0.29	0.01	0.30	0.01	0.19	0.00
MgO	4.08	0.03	4.13	0.03	4.15	0.03
CaO	12.18	0.06	12.17	0.05	9.49	0.03
Na_2O	5.63	0.10	5.47	0.09	3.50	0.09
K_2O	5.42	0.07	5.14	0.05	3.69	0.04
P_2O_5	1.48	0.03	1.47	0.03	0.66	0.02
TOTAL	98.04		98.71		98.39	
$Fe^{2+}/\Sigma Fe$	0.82	0.01	0.29	0.01	0.86	0.01
FeO	9.96	0.31	3.76	0.28	10.03	0.32
ΣFeO	12.20	0.37	12.84	0.99	11.67	0.37
Fe_2O_3	2.29	0.06	10.26	0.30	1.83	0.05
NBO/T[a]	1.01		1.01		1.01	
NBO/T[b]	0.93		0.71		0.93	
NBO/T[c]	0.57		0.55		0.56	
Density, (kg m^{-3})	2833	± 05	2833	± 04	2776	± 04
Liquidus	~1220°C		~1220°C		~1260°C	
Viscosity near liquidus	36 Pa s		30 Pa s		40 Pa s	

and nepheline (~80%) surrounding sparse, euhedral nepheline and plagioclase phenocrysts. There was no glass content observed in these slides. Vesicularity of this sample is similar to that of the 2002 eruption (~10%) since this lava flow resulted from the draining of the degassed lava lake. Density of this sample was calculated to be identical to the 2002 eruption sample within error. The two Nyiragongo samples are almost chemically identical, allowing for NYI-002 to substitute for NYI-001 when bulk

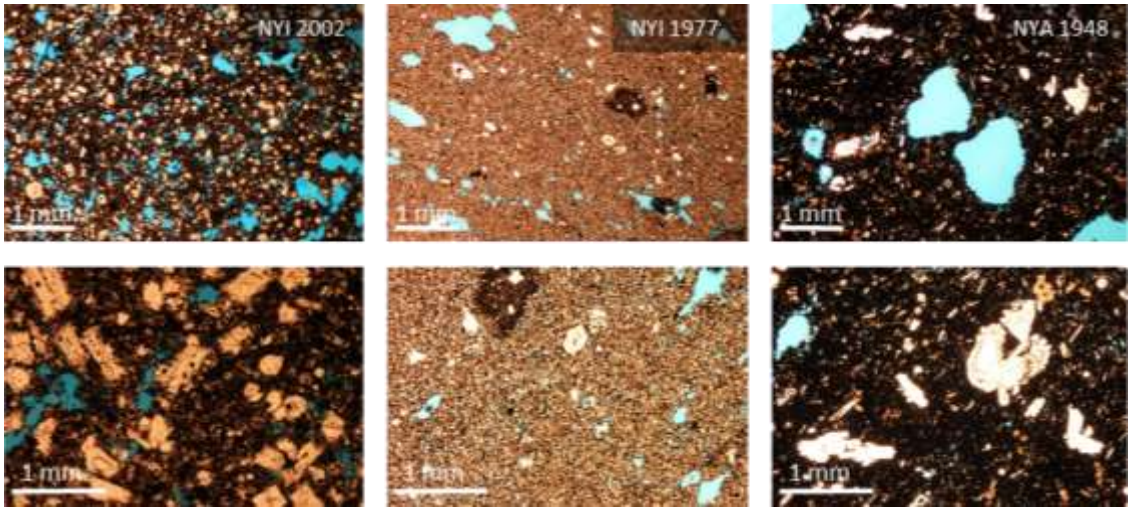

Figure 3. *Photomicrographs of original bulk rock material for NYI-001, NYI-002, and NYA-001. (left) NYI-001 overview at (top) 2x optical magnification and (bottom) 4x optical magnification in plane-polarized light. (middle) NYI-002 overview at (top) 2x optical magnification and (bottom) 4x optical magnification in plane-polarized light. (right) NYA-001 overview at (top) 2x optical magnification and (bottom) 4x optical magnification in plane-polarized light.*

material was exhausted. Due to this similar chemical composition, samples were used interchangeably between the 1977 and 2002 eruptions during experimentation as they are assumed to have the same behavior.

The 1948 Nyamuragira sample (labeled NYA-001) shows another porphyritic texture. Phenocrysts are mainly subhedral plagioclase (~25%) in a groundmass of plagioclase and pyroxene microlites (~60%). No glass was observed in this sample. Vesicularity of this sample is slightly higher than in those of Nyiragongo (~15%). This is primarily due to the persistent lava lake in the caldera of Nyiragongo that allows more degassing to occur. Density of the Nyamuragira remelted glass sample was calculated to be ~2776 ± 5 kg/m^3.

Experimental Methods

Glass synthesis

Samples were individually crushed in a steel shatter box for two minutes. The powder was then collected in a previously iron saturated Pt90-Rh10 crucible and placed in a muffle furnace where it was heated to 1600°C. To ensure homogenization, the melt was stirred regularly during the heating process. After two hours the melt was quenched on a copper plate and allowed to cool before remelting and requenching.

Parallel-plate Viscometry

Cylindrical cores (approximately 6 mm radius by 8 mm height) were drilled from the glass samples. A Theta Industries Rheotronic III parallel-plate viscometer was used to measure viscosity under uniaxial compression applied by a 1500 g load. This instrument is capable of viscosity measurements between ~10^8 and 10^{13} Pa s. A transducer is used to measure sample length to ± 0.1 μm and viscosity, η, is calculated using the relationship from Gent (1960) that assumes perfect slip, so that the sample remains cylindrical as it shortens:

(1) $$\eta = \frac{\sigma}{3(\partial\varepsilon/\partial t)}.$$

where σ is the uniaxial stress and $(\partial\varepsilon/\partial t)$ is the longitudinal strain rate. The viscometer was calibrated using National Institute of Standards and Technology (NIST) standard glasses and verified to be accurate to within 0.06 log units, with a precision based on repeat measurements of better than 0.04 log units (Whittington et al., 2009).

Concentric Cylinder Viscometry

A Theta Industries Rheotronic II Rotating Viscometer was used with a Brookfield DV3TRV Rheometer head for superliquidus experiments. This head has a spring torque value calibrated to 7.178×10^{-4} N m which in our setup is capable of measuring viscosities between 0.1 and 1000 Pa s. Instrument calibration was against Brookfield standard oils ranging from 10 to 100 Pa s. Samples were placed in a Pt90-Rh10 crucible 65 mm tall and with an internal radius of 16.075 mm. The crucible is then held by three alumina rods and lowered into a box furnace capable of operating to 1600°C. A Pt90-Rh10 sleeve with a hemispherical tip is attached to an alumina spindle, which is then lowered into the melt. The sleeve has a length of 65 mm and an external radius of 3.75 mm. A particular rotation rate is chosen and the torque required to achieve that rate is measured. Shear stress, σ, is then defined by:

(2) $$\sigma = \frac{\tau}{2\pi(R_b^2 L)}$$

where τ is the torque on the spindle, $R_b$is the radius of the spindle, and L is the immersion depth of the spindle. Immersion depth is controlled by a micrometer and actual depth is measured directly by residual melt left on the Pt90-Rh10 sleeve after each experiment. With this setup, the assembly has a wide gap geometry such that the ratio of crucible radius (R_c) to spindle radius (R_b) is approximately 4.02. This allows for crystallizing phases with large aspect ratios, such as plagioclase, to align with the flow direction. The following equation is used to calculate shear strain rate ($\dot{\gamma}$):

(3) $$\dot{\gamma} = \frac{2\omega}{n(1-(R_b/R_c)^{2/n})}$$

where ω is the angular velocity of the spindle and *n* is the flow index calculated by finding the slope of a linear regression of $\ln(\tau)$ and $\ln(\omega)$ (Stein and Spera, 1998).

Rheological constitutive relationships describe the relationship between applied stress and resulting strain rate. The simplest form of this relationship applicable to lavas is that of a Newtonian fluid:

$$\sigma = \eta\dot{\gamma} \tag{4}$$

where η is the viscosity and $\dot{\gamma}$ is the strain rate. Silicate melts behave as Newtonian fluids except at very high strain rates (Webb and Dingwell, 1990). Once crystals and/or gas bubbles are considered, experiments have shown that a linear relationship typically no longer holds (Giordano and Dingwell, 2003; Giordano et al., 2008; Sehlke et al., 2014; Sehlke et al., 2015). A more general constitutive relationship is the Herschel-Bulkley equation:

$$\sigma = \sigma_y + K\dot{\gamma}^n \tag{5}$$

where σ_y represents the initial yield strength that must be overcome before strain occurs, *K* is the consistency of the material (equivalent to the viscosity for a strain rate of 1 s^{-1}), and *n* is the flow index or power-law exponent, which describes the deviation from linearly proportional (Newtonian) behavior. A flow index greater than one implies shear-thickening behavior, and a flow index less than one implies shear-thinning behavior. Bingham materials are characterized by $n = 1$ but with a detectable yield strength.

Subliquidus rheological experiments were performed at various crystal fractions using a Brookfield HBDV-III Ultra measuring head with a stronger spring constant of 5.7496×10^{-7} N m. NIST standard glasses were used to check the accuracy of the

viscometer, which is better than 0.06 log units (Getson and Whittington, 2007). Samples were heated to 1450 °C at a rate of 5° C/min to ensure complete melting of all crystal phases. The spindle was then inserted and allowed to rotate at a constant angular velocity while the sample is cooled at 10° C/min to a target temperature below the liquidus. Once the target temperature was reached it was allowed to equilibrate overnight for 10-12 hours, until the torque stabilized for at least four hours. After the equilibration period, the strain rate was varied by changing the angular velocity at regular intervals to measure over the widest range of torque values as possible, between 0.01 to 99.99% of total spring capacity. Each segment of a particular angular velocity lasted for 45 to 60 minutes to allow for equilibration, and data were collected for 10 to 20 minutes at each stabilized period of torque readings. After all programmed segments are complete, the crucible and spindle were quenched immediately in a water bath to prevent continuing crystallization. After reaching room temperature, glass cores were drilled from the crucible and sampled at varying depths from the top to approximately 3 cm depth.

Density Determination

Densities were measured after each experiment using the Archimedean method. Sample mass was measured in air and while immersed in ethanol. Density of the sample can then be calculated using the two masses and the temperature corrected density of the ethanol. Five measurements were made on each sample as well as a standard quartz reference with a precision of ± 8.4 kg/m^3 (2σ), or better than 0.4%. Data are reported in Table 2.

Table 2. *Crystal/glass fraction, aspect ratio, rheological parameters, density, and mineralogy data summary for each NYI and NYA subliquidus experiment. Yield strengths are given for Bingham (B), power-law at a strain rate of 0.01 s^{-1} (PL), and Herschel-Bulkley (HB) models. Crystal and glass fractions were determined from BSE images.*

NYI									
Property	**Symbol**	**1221°C**	**1205°C**	**1190°C**	**1178°C**	**1168°C**	**1161°C**	**1153°C**	**1145°C**
Melt Fraction	$\Sigma\phi_m$	1.00	0.98 ± 0.02	0.96 ± 0.02	0.97 ± 0.02	0.97 ± 0.04	0.98 ± 0.02	0.95 ± 0.03	0.95 ± 0.02
Crystal Fraction	$\Sigma\phi_c$	0.00	0.003 ± 0.02	0.003 ± 0.02	0.005 ± 0.02	0.04 ± 0.04	0.03 ± 0.02	0.05 ± 0.04	0.04 ± 0.02
Mean Aspect Ratio	$\bar{R}$	--	1.42	1.42	1.8	1.71	1.91	1.81	1.7
Flow Index	n	0.94 ± 0.02	0.96 ± 0.01	0.95 ± 0.02	0.96 ± 0.04	0.78 ± 0.08	0.94 ± 0.04	0.89 ± 0.04	0.82 ± 0.04
Yield Strength (B)	$\sigma_{y(B)}$ (Pa)	14 ± 20	4 ± 1	-2 ± 2	2 ± 26	109 ± 20	-1 ± 63	4 ± 22	193 ± 170
Yield Strength (PL)	$\sigma_{y(PL)}$ (Pa)	1 ± 1	1 ± 1	1 ± 1	1 ± 1	9 ± 2	2 ± 1	2 ± 1	19 ± 2
Yield Strength (HB)	$\sigma_{y(HB)}$ (Pa)	0 ± 9	2 ± 4	30 ± 15	51 ± 37	0 ± 47	24 ± 48	0 ± 74	0 ± 49
Density	ρ (kg m^{-3})	2803 ± 02	2793 ± 02	2787 ± 01	2780 ± 03	2794 ± 01	2805 ± 04	2789 ± 02	2841 ± 03
	Mineralogy								
	Spinel	--	$Fe_{31}Mg_{69}$	$Fe_{29}Mg_{71}$	$Fe_{25}Mg_{75}$	$Fe_{24}Mg_{76}$	$Fe_{25}Mg_{75}$	$Fe_{20}Mg_{80}$	$Fe_{32}Mg_{68}$
	ϕ_c and R_i	--	0.003 1.42	0.003 1.42	0.01 1.80	0.04 1.71	0.02 1.96	0.04 1.79	0.04 1.69
	Pyroxene							$Ca_{54}Mg_{20}Fe_{26}$	$Ca_{54}Mg_{21}Fe_{25}$
	ϕ_c and R_i							0.01 2.00	0.001 1.96
NYA									
Property	**Symbol**	**1255°C**	**1235°C**	**1217°C**	**1182°C**	**1178°C**	**1174°C**	**1154°C**	
Melt Frac.	$\Sigma\phi_m$	0.99 ± 0.01	0.98 ± 0.02	0.97 ± 0.02	0.95 ± 0.06	0.97 ± 0.02	0.91 ± 0.02	0.89 ± 0.01	
Crystal Frac.	$\Sigma\phi_c$	0.001 ± 0.004	0.02 ± 0.02	0.02 ± 0.02	0.06 ± 0.06	0.03 ± 0.02	0.08 ± 0.02	0.11 ± 0.02	
Mean Aspect Ratio	$\bar{R}$	1.37	1.82	1.79	1.91	1.81	2.23	2.49	
Flow Index	n	0.89 ± 0.02	0.85 ± 0.04	0.85 ± 0.04	0.94 ± 0.10	0.88 ± 0.14	0.80 ± 0.08	0.42 ± 0.14	
Yield Strength (B)	$\sigma_{y(B)}$ (Pa)	13 ± 8	23 ± 2	75 ± 81	12 ± 82	269 ± 699	203 ± 137	694 ± 298	
Yield Strength (PL)	$\sigma_{y(PL)}$ (Pa)	1 ± 1	2 ± 1	5 ± 1	8 ± 1	12 ± 3	15 ± 2	157 ± 37	
Yield Strength (HB)	$\sigma_{y(HB)}$ (Pa)	5 ± 13	45 ± 27	0 ± 41	0 ± 84	39 ± 119	0 ± 60	0 ± 443	
Density	ρ (kg m^{-3})	2746 ± 02	2736 ± 02	2741 ± 02	2745 ± 02	2775 ± 01	2741 ± 03	2772 ± 02	
	Mineralogy								
	Spinel	$Fe_{57}Mg_{43}$	$Fe_{50}Mg_{50}$	$Fe_{48}Mg_{52}$	$Fe_{31}Mg_{69}$	$Fe_{39}Mg_{61}$	$Fe_{36}Mg_{64}$	$Fe_{40}Mg_{60}$	
	ϕ_c and R_i	0.001 1.37	0.02 1.82	0.02 1.79	0.04 1.79	0.03 1.81	0.03 1.79	0.05 1.72	
	Plag				$An_{71}Ab_{26}Or_3$		$An_{72}Ab_{25}Or_3$	$An_{69}Ab_{27}Or_4$	
	ϕ_c and R_i				0.01 4.81		0.04 3.33	0.06 3.88	

Chemical Analysis

Drilled glass cores, sampled from 2-3 cm depth in the crucible, were adhered to glass slides using a bonding agent. Two samples from each experiment were examined: one cross-sectional view (vertical/tangential, perpendicular to the flow direction) and one parallel view (horizontal/radial, parallel to the flow direction). Samples were then polished using a series of successively finer grit papers on a polishing wheel to create thin sections for microprobe analysis. The final polish was achieved with a 0.3 micron alumina paste. Chemical compositions of glass and crystals were analyzed using a JEOL JXA-8200 electron microprobe, equipped with five wavelength-dispersive spectrometers and a JEOL (e2v/Gresham) silicon-drift energy-dispersive spectrometer, located at Washington University at St. Louis. The apparatus was operating with a 15 kV accelerating potential and 25 nA probe current for all spot analyses. A 5 μm diameter electron beam was used for crystals and a 20 μm diameter electron beam was used for glasses. Silicate and oxide standards were used for calibration and data were corrected using CITZAF following Armstrong (1995). Approximately ten individual analyses are obtained for glasses and three for each crystal phase present.

Fe-Redox

Long-duration subliquidus experiments could result in a change in sample oxidation state, which may have an effect on sample viscosity (e.g. Dingwell and Virgo, 1988). We determined the redox state of Fe in the initial lava samples, the initial remelts, and the quenched products of each subliquidus experiment. Bulk iron oxidation state was measured using methods described by Wilson (1960) and Schuessler et al. (2008). A full description of our procedure can be found in Sehlke et al. (2014). Each run included 3-8

unknowns from the subliquidus experiments (a redundant measurement was made for each unknown sample), two USGS standards (BIR-1a basalt and W-2a Diabase), and a blank control. A duplicate vial was created for each sample and standard to improve the accuracy of the measurement. Between 10 and 20 mg of sample was measured into teflon vials. Each vial was filled with 2 mL of ammonium vanadate solution and 2 mL of a hydrofluoric and sulfuric acid mixture. Each vial was then heated overnight on a hotplate set at 70° C. After heating, each sample was placed in the ultrasonic bath for a 20 minutes to breakdown any solids that remain. Any Fe^{2+} in the samples was oxidized during this decomposition. Samples were then neutralized using 5 mL of hot boric acid which restored the ferrous iron content, and were then transferred into flasks containing 10 mL 2:2' bipyridine and 10 mL ammonium acetate. This produced a red-tinted complex containing only ferrous iron.

Ultraviolet/Visible (UV/Vis) photo-spectrometry was carried out with a Nanodrop1000 UV/Vis spectrometer to determine the iron concentration. Absorption spectra were taken between 420 and 720 nm with a path length of 1 mm. The 700 nm background absorbance was then subtracted from the 523 nm absorbance peak of the Fe^{2+} complex. Standard solutions of known concentrations (ranging from 0 to 56 ppm) were then used to construct a calibration curve. The Beer-Lambert law was then applied to calculate the iron concentration in each sample solution. Ferrous iron concentrations that were originally in the samples is denoted as *original* Fe^{2+}. Then, after ~10 mL of each solution has been separated and reduced by between 13-15 mg of hydroxylamine hydrochloride, all the ferric iron was converted to ferrous iron. This solution is analyzed in the Nanodrop1000 in the same way providing a measurement of the total iron content

in the sample, denoted as ΣFe^{2+}. The difference between the total iron (ΣFe^{2+}) and the ferrous iron in the sample (original Fe^{2+}) reflects the concentration of ferric iron (Fe^{3+}) in the sample. Two solutions were prepared for each subliquidus experiment and each solution was subsequently analyzed three times in the Nanodrop1000 for ferrous and ferric iron. Accuracy was checked against a blank and USGS standards BIR-1a (basalt) and W-2a (diabase) to an uncertainty of 0.20 wt% (2σ).

Crystal Volume Fraction and Aspect Ratio

Several backscattered electron images (BSE) were taken of glass and crystals at magnifications of 40x, 180x, and 2000x. These images were processed by using Adobe Photoshop® to isolate single phases present in the sample. The number of pixels were counted for each phase using the histogram function and were averaged over three calculations, each using a slightly different tolerance. This average is to account for the inexact crystal boundaries formed by the pixels. This inexactitude may result in crystal fractions and melt fraction that do not sum to 1.0 but are still within a 2σ uncertainty. Processing images at different magnifications for the same sample provides a standard deviation of 2-4 vol.% for each crystal fraction.

The freeware program ImageJ (http://imagej.nih.gov/ij/) was used to determine crystal aspect ratio by utilizing the automatic ellipse fitting procedure to the individual grain boundaries for each present phase. Each ellipse was subsequently checked for accuracy manually. Should the program be unable to adequately represent the aspect ratio with an ellipse, the following equation was used to calculate the aspect ratio by hand:

(6) $$\bar{R} = \frac{\Sigma R_i \varphi_c}{\varphi_c}$$

where R_i is the apparent mean aspect ratio of each phase and φ_c is the crystal area fraction.

Results

Liquid viscosity

Compositional data of the quenched glasses analyzed by the microprobe are summarized in Table 1. Viscosities of the anhydrous, crystal-free liquids were measured using both concentric cylinder and parallel plate viscometers to span the range of low (10^0-10^5 Pa s) to high (10^8-10^{13} Pa s) viscosities respectively. These data are presented in Tables 3a and 3b and plotted on an Arrhenian diagram in Figure 4.

Nyiragongo

Backscattered electron (BSE) images for each subliquidus experiment are presented in Figure 5a. Table 2 compiles crystal fraction, aspect ratio, and mineralogical data for each image displayed. The first experiment was done at 1221°C and no crystals were observed. The next experiment was undertaken at 1205°C and produced the first iron-magnesium spinels [$(Fe_{0.31}Mg_{0.69})(Fe_{0.86}Al_{0.13}Ti_{0.02})_2O_4$]; however, crystal fraction is only about 0.003 ± 0.02, so the liquidus is assumed at 1213 ± 7° C. Mean aspect ratio was calculated to be approximately 1.42 ± 0.42 (2σ). At 1190°C, the spinel composition remained with uncertainty of the previous experiment [$(Fe_{0.29}Mg_{0.71})(Fe_{0.86}Al_{0.12}Ti_{0.02})_2$] and no new phases formed. The crystal fraction and the mean aspect ratio did not change from the previous experiment: 0.003 and 1.42, respectively. The 1178°C experiment resulted in the spinel slightly decreasing in iron [$(Fe_{0.25}Mg_{0.75})(Fe_{0.86}Al_{0.13}Ti_{0.02})_2$] and a higher crystal fraction of approximately 0.01 ± 0.02. Again, no new phases formed and the mean aspect ratio falls within uncertainties of the previous experiments at 1.80 ±

Table 3a. *Crystal free, liquid viscosity measurements at high temperature and near the glass transition for Nyiragongo bulk material.*

Nyiragongo (NYI-001)					core 1	core 2
Temp (°C)	10,000/T (K^{-1})	log η (Pa s)	Temp (°C)	10,000/T (K^{-1})	log η (Pa s)	log η (Pa s)
1551.5	5.48	-0.09	764.5	9.64		7.93
1517.2	5.59	0.01	752.7	9.75		8.49
1469.3	5.74	0.21	738.6	9.88		9.06
1420.7	5.90	0.41	735.2	9.92	9.13	
1372.4	6.08	0.63	732.4	9.94	9.42	
1323.5	6.26	0.86	727.7	9.99	9.45	
1275.8	6.46	1.12	722.6	10.04		9.64
1228.9	6.66	1.44	722.0	10.05	9.69	
1203.8	6.77	1.78	717.1	10.10	9.89	
			712.2	10.15	10.09	
			707.6	10.20		10.21
Liquidus	1220° C		707.2	10.20	10.29	
			701.6	10.26	10.50	
TVF parameters			694.9	10.33	10.76	
A	-4.82		681.5	10.48		11.22
B	5685.14		680.4	10.49		11.19
C	601.27		674.3	10.55		11.55
			670.0	10.60	11.76	
RMSD	0.08 log Pa s		661.3	10.70		12.13

0.18. During the 1161°C experiment, spinel composition [$(Fe_{0.25}Mg_{0.75})(Fe_{0.86}Al_{0.12}Ti_{0.02})_2$] remained the same as the previous experiment; however, the crystal fraction increased to 0.02 ± 0.02. Mean aspect ratios were calculated to approximately 1.91 ± 0.18. A subsequent experiment run at 1168°C resulted in a crystal fraction of 0.04 ± 0.04 and mean aspect ratios of approximately 1.71 ± 0.64. The 1153°C experiment resulted in another slight drop in iron content of the spinel [$(Fe_{0.20}Mg_{0.80})(Fe_{0.87}Al_{0.12}Ti_{0.01})_2$]. Spinel crystal fraction is calculated to be 0.04 ± 0.04 and mean aspect ratio is 1.79 ± 0.28. This experiment was where the first pyroxenes were observed.

Table 3b. *Crystal free, liquid viscosity measurements at high temperature and near the glass transition for Nyamuragira bulk material. Red values were points omitted from the data fit due to insufficient deformation in the segment (<10 μm after relaxation).*

Nyamuragira (NYA-001)					core 1	core 2
Temp (°C)	10,000/T (K^{-1})	log η (Pa s)	Temp (°C)	10,000/T (K^{-1})	log η (Pa s)	log η (Pa s)
1591.6	5.36	0.01	771.6	9.57		8.92
1544.1	5.50	0.23	759.2	9.69		9.48
1507.7	5.62	0.35	745.8	9.81	10.18	
1459.3	5.77	0.55	745.1	9.82	9.85	
1411.0	5.94	0.77	743.2	9.84		10.23
1362.6	6.11	1.01	739.4	9.88	10.19	
1313.8	6.30	1.27	732.5	9.94	10.50	
1266.2	6.50	1.60	732.4	9.94	10.57	
			728.0	9.99		10.90
			727.9	9.99		10.96
Liquidus	1260° C		727.1	10.00	10.76	
			722.2	10.05	10.95	
TVF parameters			712.5	10.15		11.55
A	-4.45		711.4	10.16	11.38	
B	5439.03		702.5	10.25	11.78	
C	642.52		692.0	10.36		12.15
RMSD	0.10 log Pa s					

These are clinopyroxenes [$(Ca_{0.54}Mg_{0.20}Fe_{0.26})SiO_3$] that form a crystal fraction of 0.01 ± 0.02 and have a mean aspect ratio of 2.00 ± 0.20. The overall crystal fraction is 0.05 ± 0.04 and the overall mean aspect ratio is 1.81 ± 0.28. The lowest temperature successful experiment was run at 1145°C resulting in an overall crystal fraction of 0.04 ± 0.02 and overall mean aspect ratio of 1.70 ± 0.18. The composition of the spinel is much higher in Fe^{2+} than spinels in previous experiments $(Fe_{0.32}Mg_{0.68})(Fe_{0.87}Al_{0.11}Ti_{0.02})_2$ with a crystal fraction of 0.04 ± 0.02 and mean aspect ratio of 1.69 ± 0.06. The pyroxene composition was almost unchanged $(Ca_{0.54}Mg_{0.21}Fe_{0.25})$ which comprised a smaller crystal fraction than the previous experiment of 0.001 ± 0.002 and a mean aspect ratio of 1.96 ± 2.00.

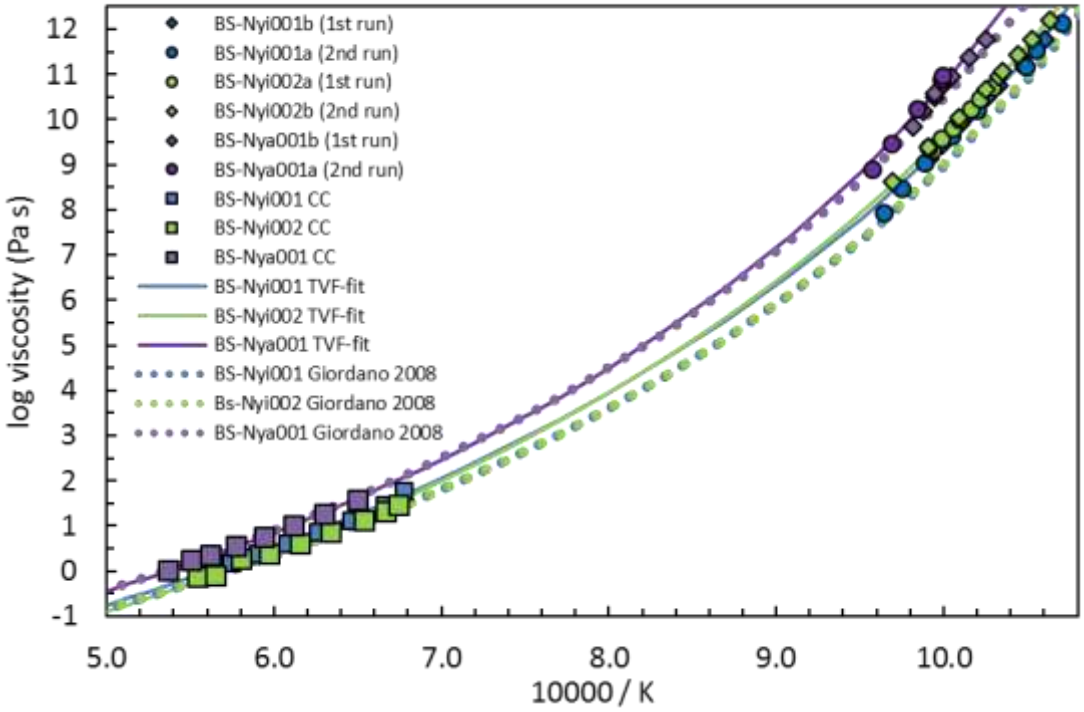

Figure 4. *Arrhenian diagram plotting viscosities for the bulk remelted material. Square points represent high temperature (superliquidus) data measured via concentric cylinder viscometry. Circles and diamonds represent low temperature (near glass transition) data measured via parallel plate viscometry. Solid curves are data from Table 3a and 3b fit using models from Vogel (1921). Dashed lines are predictions of the model from Giordano (2008).*

Nyamuragira

BSE images for each Nyamuragira experiment were also obtained and presented in Figure 5b. Table 2 compiles the crystal fraction, aspect ratio, and mineralogical data for these images. The first experiment was again at approximate liquidus conditions, which in this case is slightly above 1255°C. While this experiment resulted mostly in glass, a few iron-magnesium spinel crystals were found only amounting to a crystal fraction of $0.001^{+0.004}_{-0.001}$. These spinels are more iron-rich [$(Fe_{0.57}Mg_{0.43})$

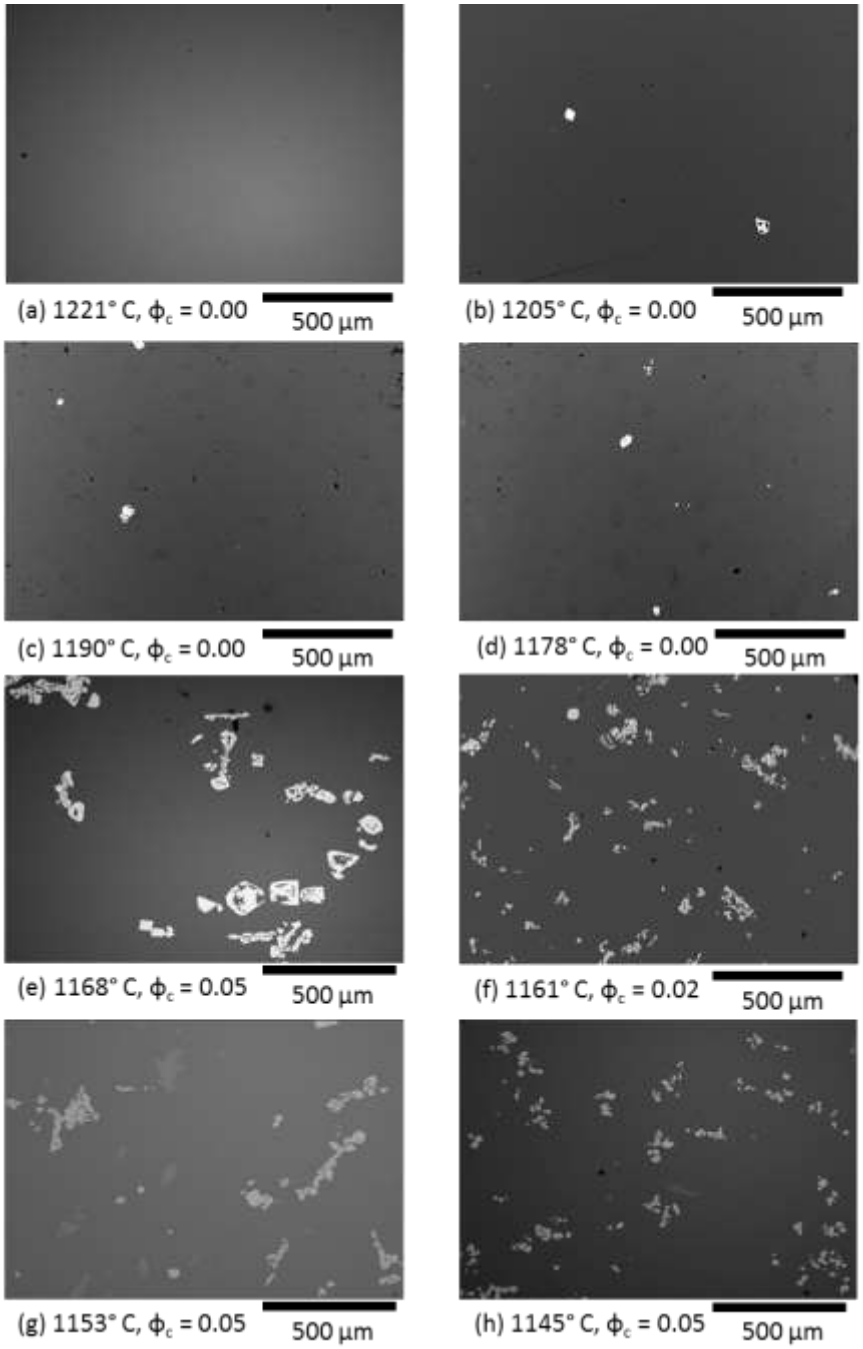

Figure 5a. *Backscattered electron images of each subliquidus experiment for Nyiragongo. No significant crystallization occurs in these samples until ~50-60°C undercooled. Oxidizing conditions suppress olivine growth and facilitate crystallization of FeMg spinels (white). Augite (light gray) begins crystallizing at 1153°C but not abundantly until lower temperatures. Crystal fraction uncertainty ± 0.02.*

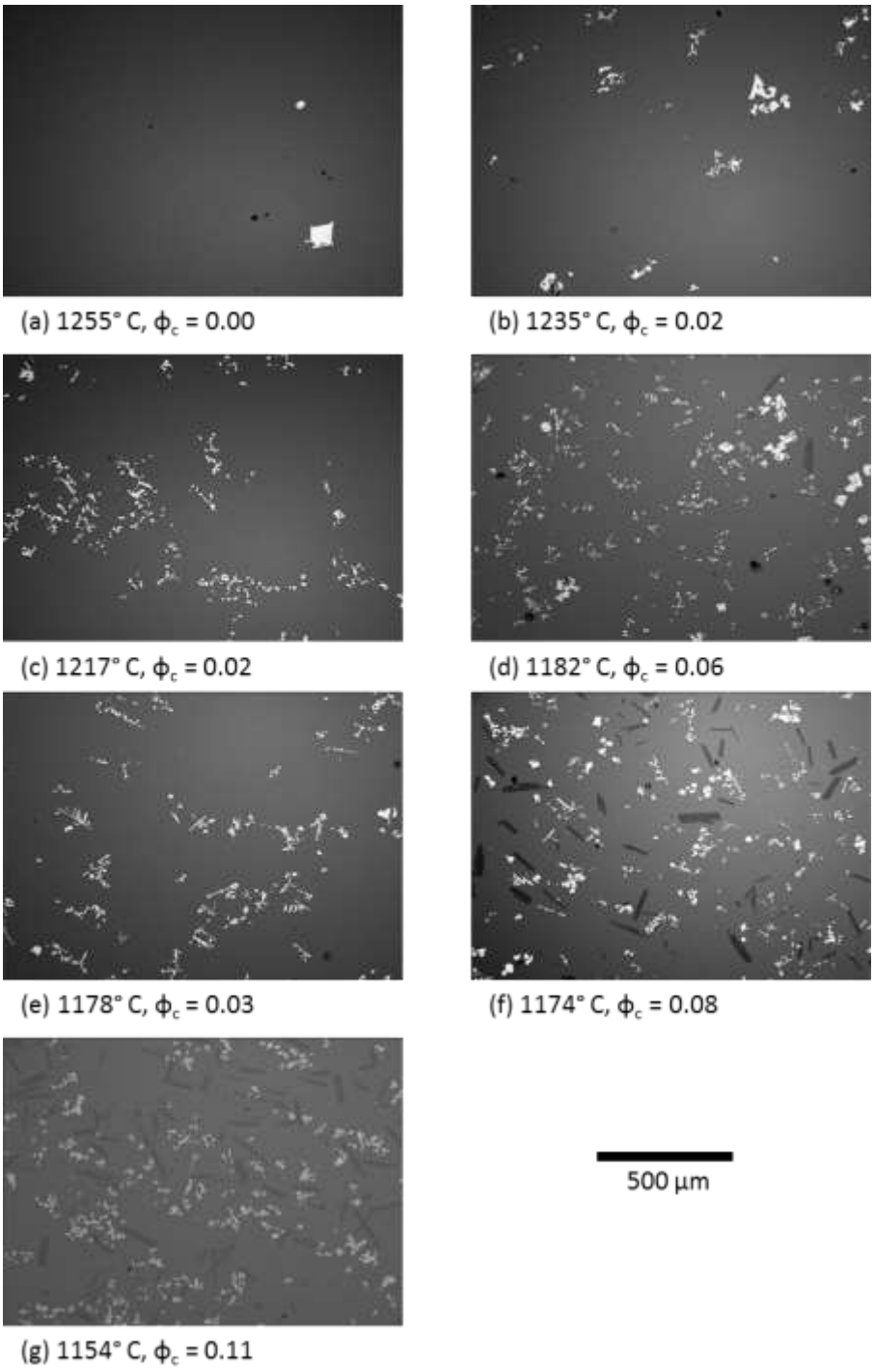

Figure 5b. *Backscattered electron images of each subliquidus experiment for Nyamuragira. Crystallization occurs over a much smaller degree of undercooling ~50-60°C undercooled. FeMg spinels (white) are the first phase to crystallize. Plagioclase (dark gray) begins crystallizing at 1182°C but not abundantly until 1174°C. Crystal fraction uncertainty ± 0.02.*

($Fe_{0.79}Al_{0.17}Ti_{0.04})_2$] than the Nyiragongo spinels and have a mean aspect ratio of 1.37 ± 0.34. The next subliquidus experiment commenced at 1235°C where crystallization is observed at a crystal fraction of approximately 0.02 ± 0.02. The spinels drop slightly in iron-content [($Fe_{0.50}Mg_{0.50}$)($Fe_{0.79}Al_{0.16}Ti_{0.05})_2$] and have a mean aspect ratio of 1.82 ± 0.06. The next experiment at 1217°C, much like the previous, resulted in a crystal fraction of only 0.02 ± 0.02, a mean aspect ratio of 1.79 ± 0.22, and a spinel composition of ($Fe_{0.48}Mg_{0.52}$)($Fe_{0.79}Al_{0.16}Ti_{0.05})_2O_4$. No new phases were detected in these samples. At 1182°C, the overall crystal fraction and mean aspect ratio was 0.06 ± 0.06 and 1.91 ± 0.40 respectively. This experiment resulted in the first appearance of plagioclase, with a crystal fraction of $0.01^{+0.04}_{-0.01}$, a mean aspect ratio of 4.81 ± 1.88, and composition of $An_{71}Ab_{26}Or_3$. The spinel phase continues to drop in iron content [($Fe_{0.31}Mg_{0.69}$) ($Fe_{0.76}Al_{0.21}Ti_{0.03})_2$] producing a crystal fraction of 0.04 ± 0.04 and a mean aspect ratio of 1.79 ± 0.12. In the successive experiment at 1178°C, the plagioclase phase is not observed. However, the spinel phase [($Fe_{0.39}Mg_{0.61}$)($Fe_{0.77}Al_{0.20}Ti_{0.03})_2$] persists forming a crystal fraction of 0.03 ± 0.02 with a mean aspect ratio of 1.81 ± 0.14. Plagioclase reappeared in the 1174°C experiment with a similar composition to the previous experiments ($An_{72}Ab_{25}Or_3$). The plagioclase forms a crystal fraction of about 0.04 ± 0.01 with a mean aspect ratio of 3.33 ± 0.98. The spinel phase [($Fe_{0.36}Mg_{0.64}$) ($Fe_{0.77}Al_{0.19}Ti_{0.04})_2$] accounts for a crystal fraction of 0.03 ± 0.01 with a mean aspect ratio of 1.79 ± 0.10. The overall crystal fraction and mean aspect ratio were calculated to be 0.08 ± 0.02 and 2.23 ± 0.18 respectively. The lowest temperature experiment successfully conducted was at 1154°C. The overall crystal fraction produced was 0.11 ± 0.02 with a mean aspect ratio of 2.49 ± 0.14. The compositions of both the spinel [($Fe_{0.40}Mg_{0.60}$)

($Fe_{0.79}Al_{0.16}Ti_{0.04})_2$] and the plagioclase ($An_{69}Ab_{27}Or_4$) did not vary significantly from the previous experiment. The spinel forms a crystal fraction of 0.05 ± 0.02 with a mean aspect ratio of 1.72 ± 0.04. The plagioclase forms a crystal fraction of 0.06 ± 0.02 with a mean aspect ratio of 3.88 ± 1.24.

Melt chemistry and evolution

As experiments decrease in temperature, crystal fraction increases, melt fraction decreases, and the residual liquid composition becomes more silicic and less iron-rich (Figure 6). For both Nyiragongo and Nyamuragira samples, FeO content drops significantly in successive experiments of decreasing temperature. This is due to the iron in the spinels that form at the liquidus and continue crystallizing at higher crystal fractions. The iron content decreases more steeply at first as the spinel is the only phase forming but decreases more shallowly at lower temperatures as the spinel become less iron-rich. While magnesium is also incorporated into the spinels, the decrease is much less dramatic because of the smaller concentration of magnesium in the solid phase. The spinels do become slightly more magnesium-rich as temperature decreases. The more dramatic decrease seen in the Nyiragongo trend is due to the incoming clinopyroxene at the lower temperatures. In the CaO curves for each composition, a slight increase followed by a slight decrease is observed. The increase is due to the spinel formation which does not incorporate much Ca, effectively enriching the melt. The successive decrease is due to the formation of augite in the lower temperature Nyiragongo samples and a calcium-rich plagioclase phase in the Nyamuragira samples. The alkalis also show a steady increase with decreasing temperature as they are not highly incorporated in the

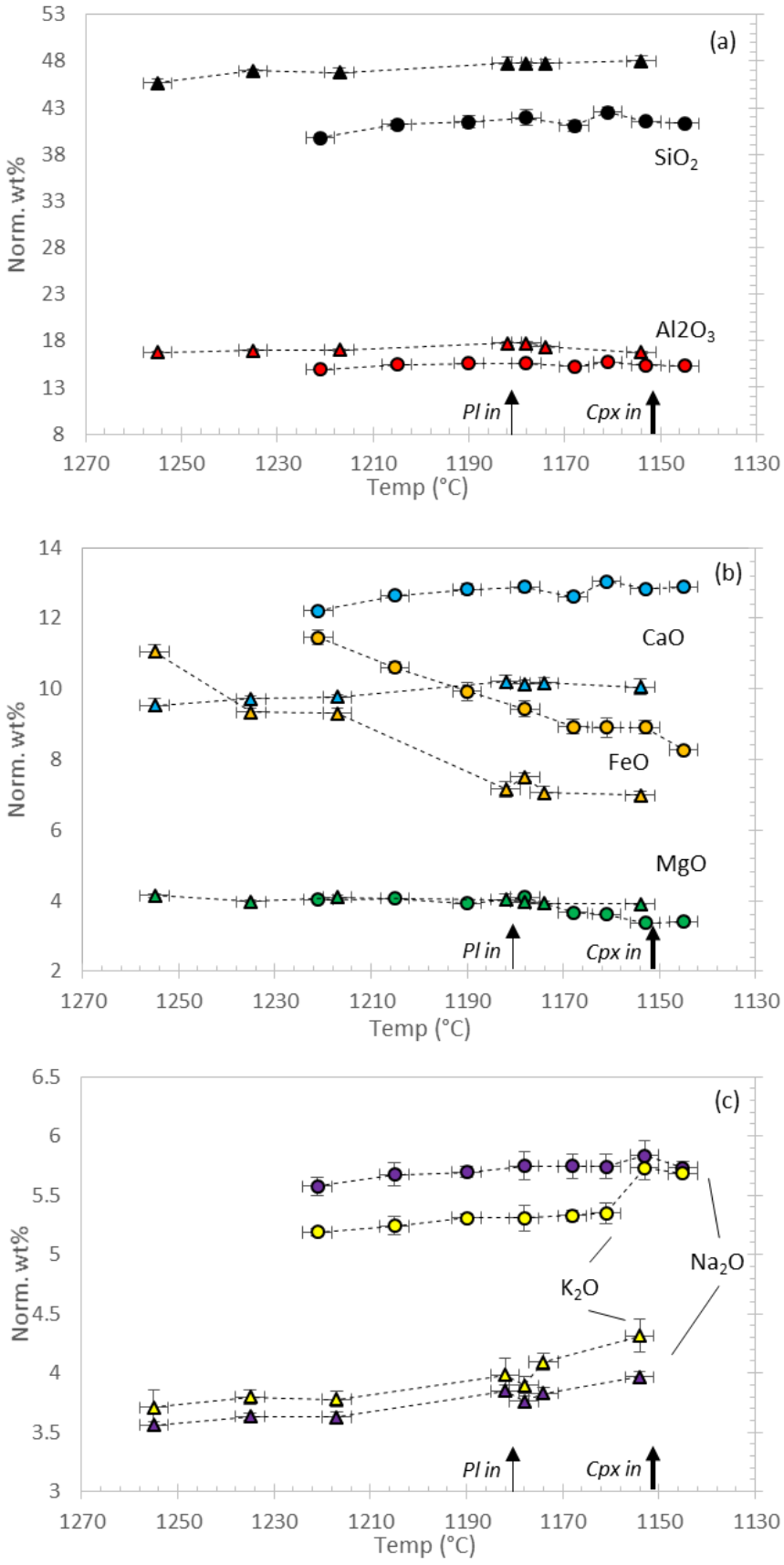
(a)
SiO2
Al2O3
Pl in
Cpx in
Norm. wt%
Temp (°C)
(b)
CaO
FeO
MgO
Pl in
Cpx in
Norm. wt%
Temp (°C)
(c)
K2O
Na2O
Pl in
Cpx in
Norm. wt%
Temp (°C)

Figure 6. *Melt chemistry evolution for Nyiragongo (circles) and Nyamuragira (triangles) compositions. (a) SiO_2 (black) and Al_2O_3 (red), (b) CaO (blue), FeO (orange), and MgO (green); (c) Na_2O (purple) and K_2O (yellow). In both cases, as temperature decreases: alkalis increase steadily, silica content increases gradually, MgO and FeO contents decrease steadily due to the crystallization of FeMg spinels, and CaO and Al_2O_3 contents slightly increase before beginning to decrease when a clinopyroxene (NYI) or plagioclase (NYA) phase begins to crystallize near the bottom of the experimental temperature range (marked by a bold arrow and narrow arrow respectively).*

crystallizing phases. Melt evolution for Nyiragongo and Nyamuragira show similar trends over the range of experimental temperatures.

Two-phase rheological properties

The flow index (n) was determined from the slope of a plot of $\ln(\sigma)$ versus $\ln(\dot{\gamma})$ for each subliquidus experiment (Figure 7). Linear regression parameters and error are reported in Table 4. Both compositions behave as Newtonian fluids ($n = 0.98 \pm 0.01$) above the liquidus. As the liquidus is crossed and the first crystals begin to form, the flow index begins to decrease where a non-Newtonian, pseudo-plastic behavior ($n < 0.95$) is observed. Nyiragongo, however, continues to exhibit near-Newtonian behavior (n between 0.94-0.96) at nearly 50°C below the liquidus temperature due to the lack of significant crystallization over that temperature range. The exception to this is the 1168°C experiment which anomalously drops to $n = 0.78 \pm 0.08$ with a crystal fraction of only 0.04 ± 0.04. This experiment falls below the trend of the other experiments albeit by a small margin. The flow index jumps back up in the following experiment at 1153°C where the $n = 0.89 \pm 0.04$. The decreasing trend observed in flow index over the lowest

two temperatures corresponds to the incoming clinopyroxene phase. At over 60°C undercooled, the crystal fraction still has not increased above 0.05 ± 0.02 achieved at the

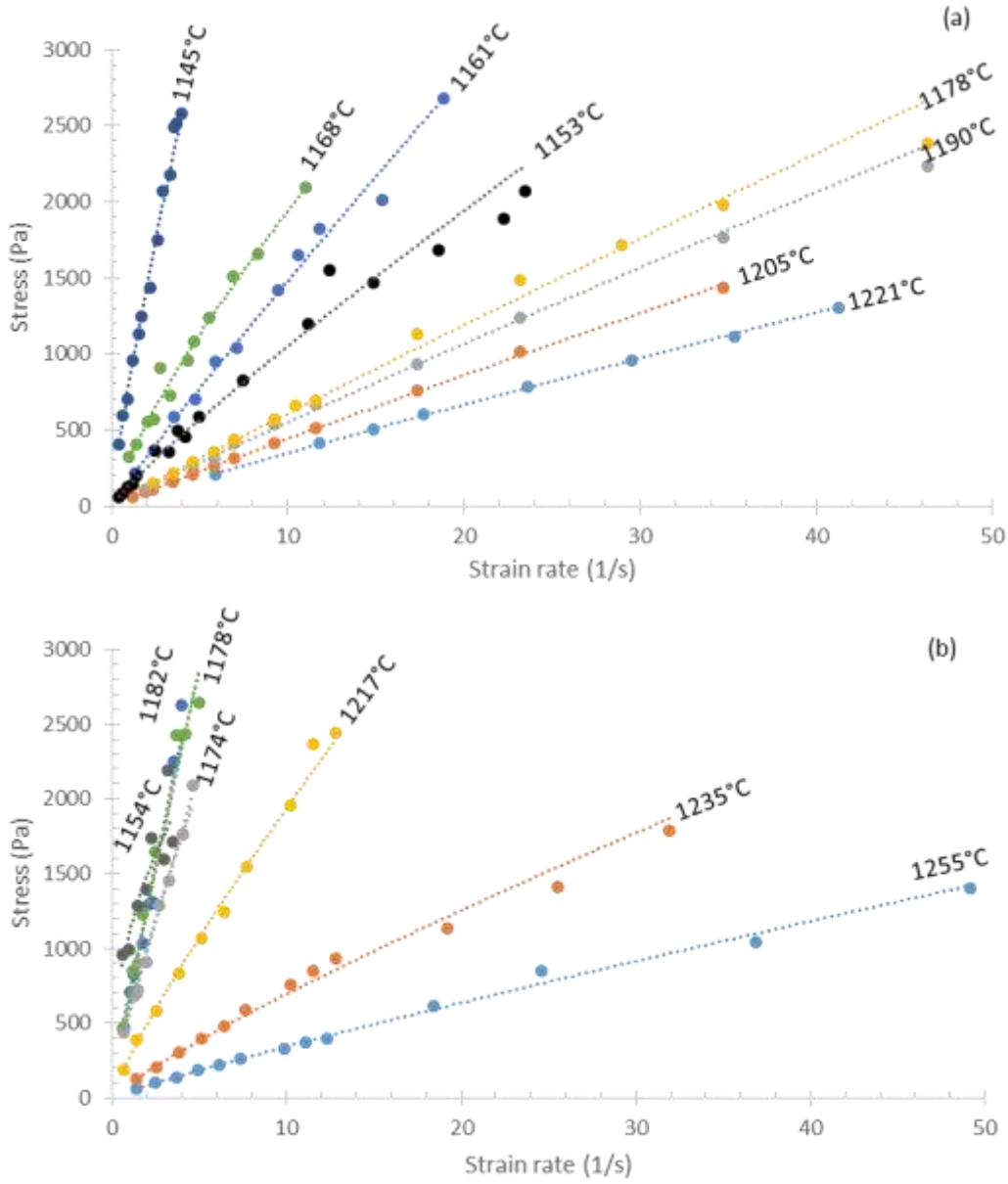

Figure 7. *Flow curves of each isothermal, subliquidus experiment plotted for (a) Nyiragongo and (b) Nyamuragira. Power law fits were calculated using the equation* $\sigma = K\dot{\gamma}^n$. *Parameters are listed in Table 4.*

Table 4. *Power law fluid parameters for Nyiragongo and Nyamuragira two-phase suspensions at each experimental temperature obtained by linear regression of ln(σ) and ln(γ̇). Flow curves are calculated by the equation* $\sigma = K(\dot{\gamma})^n$.

Property	Symbol	Temperature							
NYI		**1221°C**	**1205°C**	**1190°C**	**1178°C**	**1168°C**	**1161°C**	**1153°C**	**1145°C**
Flow Index	n	0.94 ± 0.02	0.96 ± 0.01	0.95 ± 0.02	0.96 ± 0.04	0.78 ± 0.08	0.94 ± 0.04	0.89 ± 0.04	0.82 ± 0.04
PL Consistency (Pa s)	K	40	49	61	67	321	171	137	825
HB Consistency (Pa s)	K	40	49	58	63	323	168	132	833
PL Regression Quality	R^2	0.9994	0.9999	0.9983	0.9967	0.9751	0.9961	0.9926	0.9933*
NYA		**1255°C**	**1235°C**	**1217°C**	**1182°C**	**1178°C**	**1174°C**	**1154°C**	
Flow Index	n	0.89 ± 0.02	0.85 ± 0.04	0.85 ± 0.04	0.94 ± 0.10	0.88 ± 0.14	0.80 ± 0.08	0.42 ± 0.14	
PL Consistency (Pa s)	K	44	98	273	658	692	581	1109	
HB Consistency (Pa s)	K	44	91	277	672	677	586	1118	
PL Regression Quality	R^2	0.9983	0.9940	0.9973	0.9858	0.9665*	0.9820	0.8515	

* - Regression quality for NYI 1145 and NYA 1178 is higher for the linear fit (0.9940; 0.9669) than with the power law fit. However, all data are best fit by a Herschel-Bulkley model

lowest experimental temperature of 1145°C. The flow index only reached 0.82 ± 0.04 at this temperature, which was the limit of successful experiments before the surface crust formed.

Crystal fraction begins increasing much sooner with decreasing temperature for the Nyamuragira samples. At ~25°C below the liquidus the first significant crystallization occurs where FeMg-spinels account for almost 0.02 ± 0.02 crystal fraction. Pseudo-plastic behavior is observed almost immediately (1255°C, $n = 0.89 \pm 0.02$) without the period of near-Newtonian behavior observed in the Nyiragongo lavas. The flow index then decreases slightly at 1235°C ($n = 0.85 \pm 0.04$) and remains stable within uncertainties over the next ~55°C. The flow index decreases significantly from 0.88 to 0.42 over the range of 1178°C to 1154°C which corresponds to the same range where the plagioclase phase begins crystallizing. A much higher crystal fraction is attainable (0.11

± 0.02; about twice that of the highest Nyiragongo sample) with this lava before the limitations of the instrument are reached.

Several attempts at lower temperatures were made with very limited success. While measuring at temperatures below ~1145°C is possible (down to at least 1112°C), the development of a crust on the melt surface at this temperature limits the quantifiable rheological results. This crust (~0.5-1 mm thick) forms a more rigid layer that does not flow in the same manner as the melt and thus, the measurement no longer accurately reflects the sample viscosity. The presence of surface lobate structures (Figure 8) show that this crust is still able to flow but it is no longer homogenous with the rest of the melt. When this surface layer interacts with the viscometer spindle (friction), the torque required to maintain the strain rate, and thus the viscosity readings, are artificially higher. Inversely, if there is any slip between this surface structure and the spindle (no interaction), the torque values and resulting viscosities will be artificially lower.

Figure 8. *Lobate surface structures observed in quenched concentric cylinder run products may suggest yield strength development. These surface structures are only observed at the lower temperature experiments. Examples are given above for structures found in both Nyiragongo (right, 1145°C) and Nyamuragira (left, 1165°C) compositions.*

Alternatively, this crust can also attach to the spindle itself and rotate along with it. This changes the effective dimensions of the spindle as well as the geometry of the apparatus to where it is no longer a wide gap geometry. The resulting stress and strain rate data are severely scattered and do not form a flow curve making rheological interpretation impractical.

Yield strength

No significant crystal framework was observed in any of the Nyiragongo experiments since only a small crystal fraction was achievable. However, lobate surface structures (not to be confused with the melt surface crust) were observed at 1145°C experiment (Figure 8), which have been correlated to yield strength development by Sehlke et al. (2014). In that study, surface structures were observed when crystal networks form at or above a crystal fraction 0.30. In the present work, it was found that these surface structures may form at much lower crystal fractions and with more sparse crystal networks. More crystallization is observed over the range of Nyamuragira experiments with a significant crystal framework of plagioclase and spinel developing near 1182°C (Figure 5b). This temperature is also where the plagioclase phase first begins to come in concurrently with the spinels. Surface structures were observed for this composition in the 1154°C experiment but were also found in several failed experiments between the temperatures of 1170°C and 1150°C.

Once a crystal network begins to form, a minimum stress (yield strength) may be required to overcome the resistance of this network to flow. This yield strength (σ_y) was estimated as the nonzero, y-intercept of the flow curve (Figure 7) on the stress axis (Kerr

and Lister, 1991). Due to the time constraints of making measurements at strain rates approaching 0 s^{-1}, the line estimate function was used to extrapolate from the lowest data points. Because this linear fit represents a Bingham rheological behavior, yield strength estimates are maxima for each experiment. For the Nyiragongo lavas, Bingham yield strength estimates are all within error of zero with the exception of the 1168°C and 1145°C experiments which resulted in estimates of 109 ± 20 Pa and 193 ± 170 Pa respectively (Figure 9). Similarly, the results for Nyamuragira lava are mostly within error of a zero yield strength or very nearly zero. The 1235°C experiment (ϕ_c = 0.02 ± 0.02) has a slightly higher yield strength estimate (σ_y = 23 ± 2 Pa) than the surrounding experiments. The highest crystal fraction experiment (1154°C; ϕ_c = 0.11 ± 0.02) resulted in a yield strength estimate of 694 ± 298 Pa. Although a crystal network begins forming at ~1182°C, a yield strength does not seem to develop until higher crystal fractions are achieved (starting with 1174°C: 203 ± 137 Pa). Since the rheological behavior is much more pseudo-plastic than Newtonian or Bingham, yield strength estimates were also made by calculating the stress using a power law fit at low strain rates of 0.01 s^{-1}. A similar approach was adopted by Sehlke et al. (2014), and is intended to represent the effective yield strength for a lava flow that is about to stop moving. For both lavas, at all investigated temperatures, values are much lower than Bingham estimates with only the highest crystal fraction (NYA 1154°C; ϕ_c = 0.11 ± 0.02) exceeding 20 Pa s (Figure 9). Yield strength estimates using a power law are reported in Tables 2a and 2b.

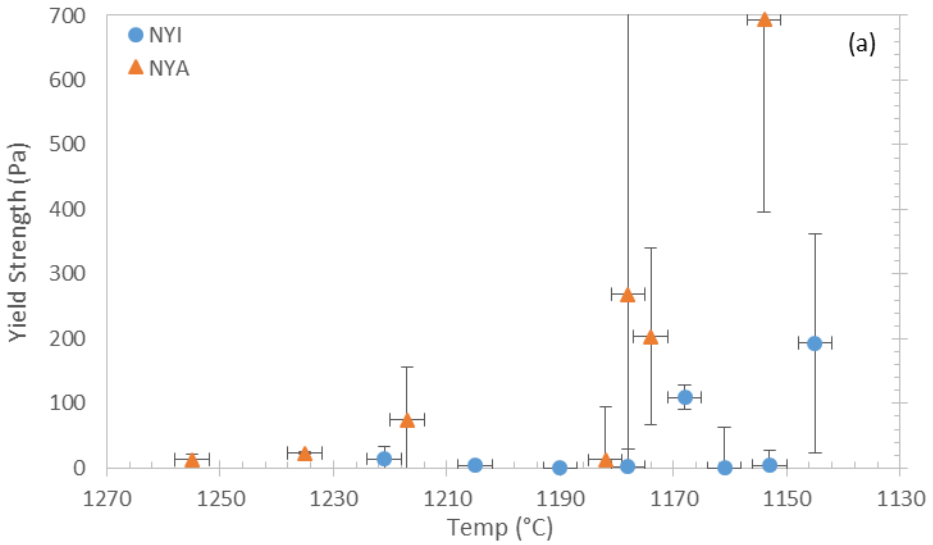
NYI
NYA
(a)
Yield Strength (Pa)
700
600
500
400
300
200
100
0
1270
1250
1230
1210
1190
1170
1150
1130
Temp (°C)

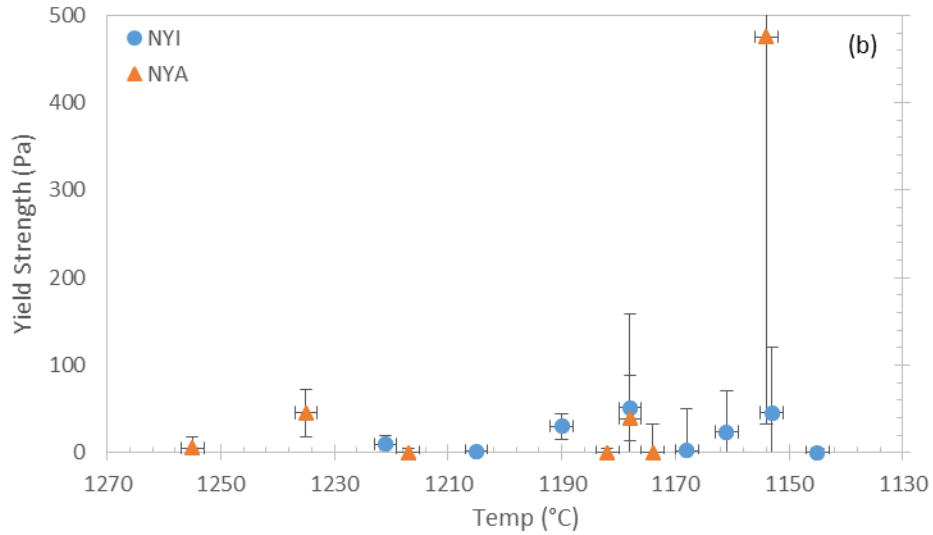
NYI
NYA
(b)
Yield Strength (Pa)
500
400
300
200
100
0
1270
1250
1230
1210
1190
1170
1150
1130
Temp (°C)

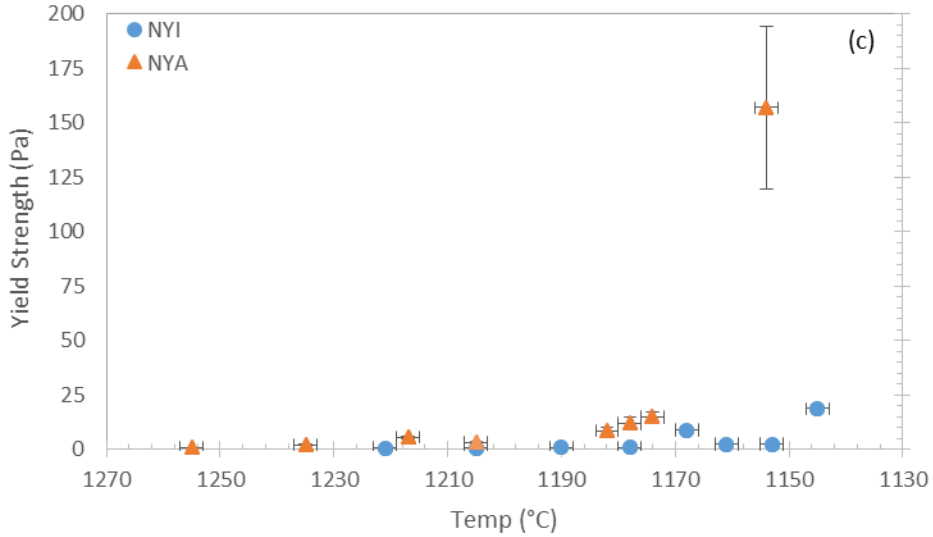
NYI
NYA
(c)
Yield Strength (Pa)
200
175
150
125
100
75
50
25
0
1270
1250
1230
1210
1190
1170
1150
1130
Temp (°C)

Figure 9. *Yield strength estimates for Nyiragongo (blue circles) and Nyamuragira (orange triangles). (a) Linear estimation using a Bingham model; (b) effective yield strength estimated by power-law model at a strain rate of 0.01* s^{-1}*; (c) yield strength estimates using a Herschel-Bulkley model. Note changes in scale.*

Discussion

Estimation of liquidus temperatures

From calorimetry data, the liquidus temperature for Nyiragongo was expected to be around 1220°C. Experimentally, the liquidus temperature is bracketed between experiments at 1221°C (completely glass) and the 1205°C ($\phi_c = 0.003 \pm 0.003$; visual confirmation of crystals from SEM images), thus, constraining the true liquidus to 1213°C ± 8°C. Calorimetry data provided an expected liquidus of 1260°C for Nyamuragira. From our experiments we know the liquidus must be near, but above, 1255°C from the minuscule crystal fraction observed ($\phi_c = 0.001 \pm 0.004$; visually confirmed from SEM images). The rhyolite-MELTS program (established by Ghiorso and Sack (1995), recalibrated by Gualda et al. (2012)) was used to model the liquidus of each composition. For oxygen fugacities (fO_2) buffered at +7 NNO, the liquidi are both calculated at well over 2000°C. In this case, it is assumed that the material retains its reducing oxygen fugacity. Appropriate liquidi are calculated at fO_2 of -0.68 and +0.75 NNO for Nyiragongo and Nyamuragira respectively.

Rhyolite-MELTS was also used to compare the observed crystallization characteristics (crystal fraction, and phase compositions) with those modeled by the program. Figure 10 shows the plots of calculated and observed cooling histories under "effective fO_2" conditions. The program accurately portrays what is observed in the Nyiragongo samples. There is very little crystallization that takes place prior to between 40 - 60°C of undercooling. Crystal fractions of about $\phi_c = 0.05$ are achieved prior to the rheological measurement limit, which is clearly seen on these graphs as a sharp increase

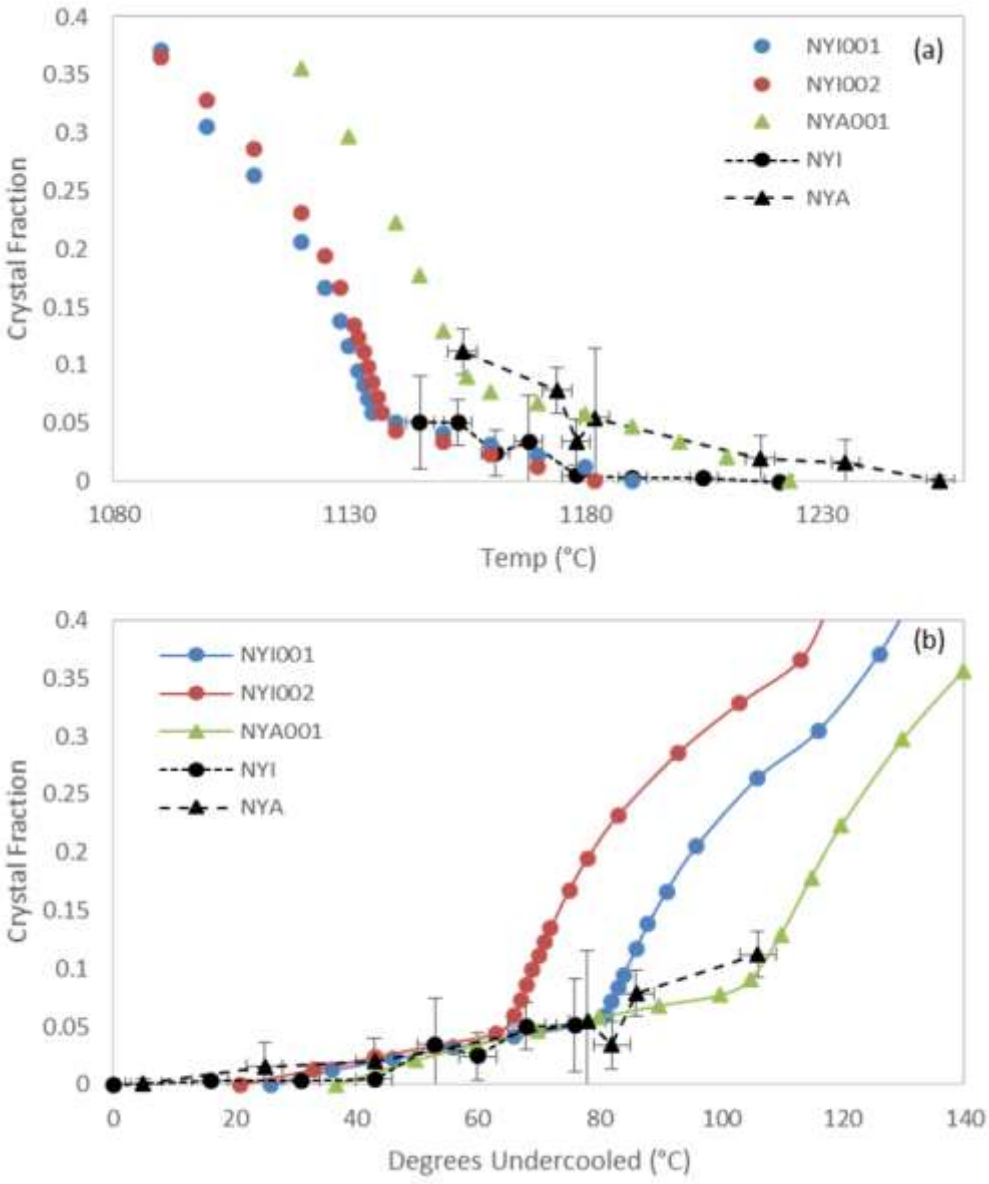

Figure 10. *Crystallization histories for Nyiragongo (circles) and Nyamuragira (triangles). The colored lines are the data calculated for NYI-001 (blue), NYI-002 (red), and NYA-001 (green) bulk material using the rhyolite-MELTS program (Gualda et al., (2012). Curves are constructed assuming an "effective fO_2" of -0.68 and +0.75 NNO for Nyiragongo and Nyamuragira respectively. The black lines are the observed crystallization data from the subliquidus experiments. (a) Data plotted against temperature for calculated and observed values. (b) Data plotted against the amount of undercooling for a more direct comparison.*

in slope. During this period, an iron-magnesium spinel is the only phase that forms (both in the lab and in the model). The experimental samples plot nicely along the calculated curves, terminating at the rapid influx of clinopyroxene where continued measurement was impractical. Augite crystals also are in good agreement compositionally between the observed and calculated values. The Nyamuragira samples follow the modeled trend just as well as the Nyiragongo sample (assuming the "effective fO_2"). The calculated curve shows a dramatic increase in crystal fraction near the 100°C undercooling point (about the same order of magnitude as the rapid increase of clinopyroxenes in the Nyiragongo calculation).

The experimental Nyamuragira samples follow the gradual increase in crystal fraction very nicely, right up until the rapid increase which signifies the limit of measurability. These samples crystallize to a very small degree over the temperature range of experiments (~100°C) yet about twice as much as the Nyiragongo samples. Again, iron-magnesium spinels are the first phase to form and show agreement in composition between observed and calculated values. However, the next phase expected to come in would be a clinopyroxene similar in composition to those found in Nyiragongo, but no augite crystals were observed in the subliquidus samples. Instead, plagioclase was the next phase observed while the calculation predicted the first plagioclase phase to form ~15°C after the augite first appears.

With such a depolymerized composition as Nyiragongo, rapid crystallization might be expected. Taking into account the duration of the experiment (~10-12 hour equilibration period at target temperature followed by 10-12 hours of isothermal measurement), we assume that an equilibrium crystal fraction is achieved. The question

of crystal settling leads to the utilization of a mass balance calculation in order to corroborate the visual analysis done by SEM. Potassium concentrations are used for the calculation since K does not incorporate into the spinel phase and can be assumed to be perfectly incompatible. Table 5 shows that the calculated glass fractions are in agreement within error of visual observations (Figure 5a). Similarly, glass fractions calculated in this manner agree within error of those determine visually (Figure 5b) for Nyamuragira. The calculation breaks down, however, when the plagioclase phase appears and potassium is no longer perfectly incompatible.

Table 5. *Mass balance calculations of glass fraction compared to visual analysis of SEM imaging for Nyiragongo and Nyamuragira subliquidus experiments. The calculation was done using potassium concentrations in the melt. The calculations are not deemed to be accurate after the clinopyroxene and plagioclase phases form.*

	Temp	Mass Bal. Gl Frac	SEM Gl Frac	(2σ)		Temp	Mass Bal. Gl Frac	SEM Gl Frac	(2σ)
NYI					***NYA***				
	1221	0.99	1.00	± 0.002		1255	0.99	0.99	± 0.01
	1205	0.98	1.00	± 0.02		1235	0.97	0.98	± 0.02
	1190	0.97	1.00	± 0.004		1217	0.98	0.97	± 0.02
	1178	0.97	0.99	± 0.01	*plag in->*	1182	0.93	0.95	± 0.06
	1168	0.96	0.97	± 0.04		1178	0.95	0.96	± 0.02
	1161	0.96	0.98	± 0.01		1174	0.96	0.91	± 0.02
cpx in->	1153	0.90	0.95	± 0.03		1154	0.86	0.89	± 0.01
	1145	0.90	0.97	± 0.02					

Effect of redox state on sample properties

Iron may have different roles in the crystal structure depending on oxidation state. The usual assumption is that ferrous iron (Fe^{2+}) acts as a network modifier while ferric iron (Fe^{3+}) can act as a network former, although both ions can potentially adopt either

role (see review by Mysen and Richet, 2005). The different coordination numbers adopted by iron atoms will affect the magma viscosity differently and therefore, oxidation state becomes important in determining how viscosity changes as the melt chemistry evolves. However, Chevrel et al. (2014) found that the difference between liquid viscosities for alkalic iron-rich basalts measured in air and at low oxygen fugacities (ΔQFM -3) was only between 0.01 and 0.02 log units. These compositions are rather similar to those of the Nyiragongo and Nyamuragira lavas, and thus redox state is not expected to affect the melt viscosity significantly in these experiments. It may, however, affect both the temperature of crystallization and the crystallizing assemblage. Duration of the natural lava flows last on the order of several hours to over a day and our experiments remain at temperature for nearly 24 hours. Remaining at the experimental temperatures on a similar time scale as the actual lava flow should ensure that any effects from oxidation would be the same.

All oxidation state information is reported in Tables 1 and 6. The Nyiragongo bulk compositions (NYI-001 and NYI-002) show a marked dichotomy in oxidation state. This may be due to the persistent lava lake activity typical of Nyiragongo. The 1977 eruption of Nyiragongo (NYI-002) drained the lava lake that had existed for decades. Being in contact with the air would have allowed these lavas to be much more oxidized than the lavas of the 2002 eruption (NYI-001). Both samples have similar FeO wt. % as measured by EPMA and UV/Vis spectroscopy varying by only ~0.50 wt. % (Table 1). However, the sample from the 1977 eruption (NYI-002) is significantly more oxidized ($Fe^{2+}/\Sigma Fe$: 0.29 ± 0.01) compared to the 2002 eruption (NYI-001; $Fe^{2+}/\Sigma Fe$: 0.82 ± 0.01). Nyamuragira has a similar Fe-content at 11.62 ± 0.10 wt.% and shares a similar oxidation

state as the 2002 Nyiragongo eruption ($Fe^{2+}/\Sigma Fe$ ratio: 0.86 ± 0.01) showing a low amount of oxidation.

The quenched experimental samples are all at least as oxidized as the bulk NYI-002 material, although the total iron contents of the wet chemistry for many of the samples are much lower than observed in totals from EPMA analyses (Table 1).

Table 6. *Iron oxidation state for each subliquidus experiment calculated following Kress and Carmichael (1991). Fe_2O_3 is listed in wt.% Fe_2O_3, not in wt.% FeO.*

Temp (°C)	FeO wt%	2σ	Fe_2O_3 wt%	2σ	ΣFe wt%	Fe^{2+}/Fe^{3+}	Fe^{3+}/Fe^{2+}
NYI							
1220	1.33	0.20	11.39	0.36	12.72	0.26	3.85
1205	1.09	0.22	10.45	0.35	11.54	0.23	4.32
1190	0.93	0.27	9.89	0.37	10.82	0.21	4.78
1178	0.83	0.26	9.47	0.39	10.29	0.19	5.16
1168	0.76	0.27	9.26	0.38	10.02	0.18	5.48
1161	0.71	0.30	9.03	0.42	9.74	0.17	5.74
1153	0.68	0.28	9.23	0.41	9.90	0.16	6.14
1145	0.60	0.22	8.69	0.45	9.30	0.15	6.47
NYA							
1254	4.95	0.28	6.10	0.32	11.05	0.43	2.35
1235	2.69	0.24	6.65	0.35	9.34	0.37	2.70
1217	2.47	0.26	6.84	0.37	9.31	0.34	2.97
1182	2.29	0.29	4.86	0.33	7.15	0.26	3.81
1178	2.36	0.29	5.14	0.42	7.50	0.26	3.82
1174	2.49	0.26	4.24	0.39	6.73	0.25	3.98
1154	2.71	0.28	4.28	0.47	6.99	0.22	4.60

Consequently, no more details can be resolved regarding oxidation state without reanalysis of the wet chemistry. Instead, the redox state of each sample was calculated following the method of Kress and Carmichael (1991). Table 6 compiles the results of these calculations for each subliquidus experiment.

Magma flow laws and yield strength

The flow indices calculated for the Nyiragongo experiments are very close to 1.0 (Newtonian behavior) for the first four subliquidus experiments covering ~60°C of undercooling (*n* ranging from 0.96 to 0.94). Successive subliquidus experiments show a more dominant pseudo-plastic behavior ($n < 0.95$) as temperature decreases and crystal fraction increases. Shear-thinning is exhibited in this rheological regime where higher strain rates produce lower apparent viscosities. The Herschel-Bulkley model (equation 5) is used as a best approximation of the flow curves (Figure 7) while still allowing for a yield strength. Yield strength estimates using the Herschel-Bulkley equation are reported in Table 2. Calculated yield strengths for Nyiragongo experiments were within uncertainty of zero, except for the 1178°C experiment, for which the best fit flow curve has a calculated yield strength of only 51 ± 37 Pa.

The results for Nyamuragira are qualitatively similar, with the power law exponent always being lower than for Nyiragongo, but always remaining above 0.85 until 1178˚C. For the lowest temperature experiments, *n* drops abruptly to 0.80 ± 0.08 at 1174˚C and 0.42 ± 0.14 at 1154˚C. The large error bars arise from the very limited range of strain rates that could be achieved at the lowest temperature. Similarly, the calculated yield strength remained close to zero until the lowest temperature experiment, with 476 ± 443 Pa at 1154˚C (Table 2). Again, a Bingham model produces a better fit quality for two lower temperature experiments. These data suggest that yield strengths are essentially undetectable (i.e. <<100 Pa) until higher crystal fractions are achieved at larger degrees of undercooling, and that lavas from both volcanoes remain very fluid for at least 50°C and perhaps 80-100˚C below their liquidus temperatures.

In Figures 11 and 12, results are compared with those of previous experimental studies of other basaltic compositions. Figure 11 shows the flow index for these compositions plotted with those from other studies. For these compositions, flow index decreases as crystal fraction increases. In general, this holds true for Nyiragongo and Nyamuragira compositions as well. While Nyiragongo may not show this trend immediately upon undercooling, the trend can be observed once significant crystallization begins (albeit without a dramatic change since only low crystal fractions were achieved). Nyamuragira shows a more pseudo-plastic behavior but follows a similar trend of little variation until a rapid decrease of *n* near the experimental limit of measurement.

Estimations of yield strength are plotted in Figure 12 along with data from previous studies. At such low crystal fractions, all yield strength estimates are within a 2σ uncertainty of zero with exception for the highest crystal fraction Nyamuragira experiment. Yield strengths may, however, develop beyond the measurement limitations (higher crystal fractions and lower temperatures). Ishibashi and Sato (2010) analyzed subliquidus data on a basalt from Fuji using a Bingham model where the y-axis intercept is the yield strength. Alternatively, Sehlke et al. (2014) determined an "effective yield strength" for a power-law fit by calculating the stress at an arbitrary, low strain rate of 0.01 s^{-1}. Soldati et al. (2015) determined their data were fit best by a power-law equation with no yield strength. Yield strengths for analog suspensions have been plotted as well. Hoover et al. (2001) determined the effects of spherical or prismatic particles on yield strength development. The combined results of all these studies show that Bingham

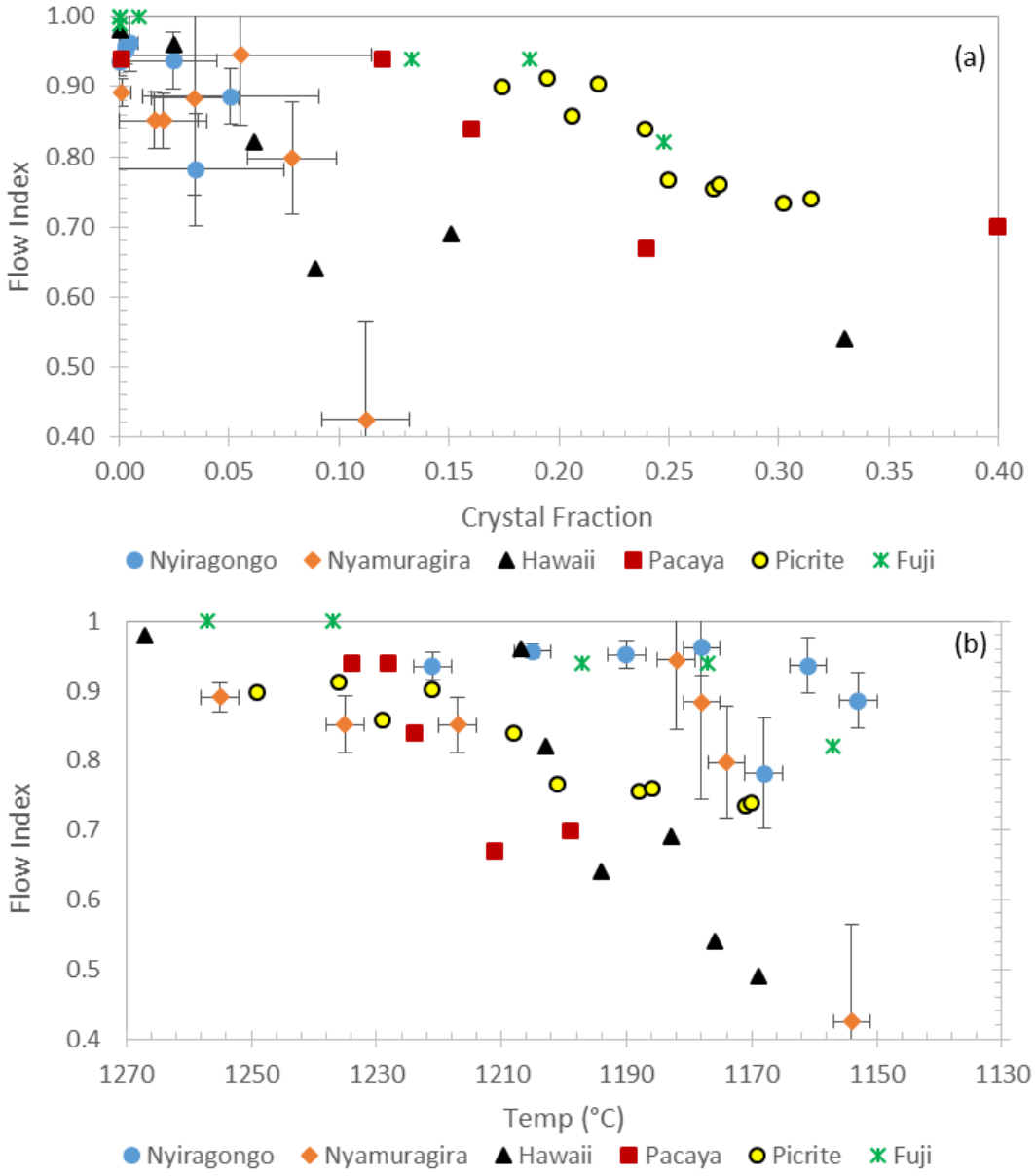

Figure 11. *(a) Flow index for Nyiragongo (blue circles) and Nyamuragira (orange diamonds) plotted along with flow indices from previous studies. The black triangles (Hawaii) are from Sehlke et al. (2014); the red squares (Pacaya) are from Soldati et al. (2015); the yellow circles (Picrite) are from Ryerson et al. (1988); the green asterisks (Fuji) are from Ishibashi (2009). (b) Data are also plotted from our study against temperature due to a small total crystal fraction narrowing the data range.*

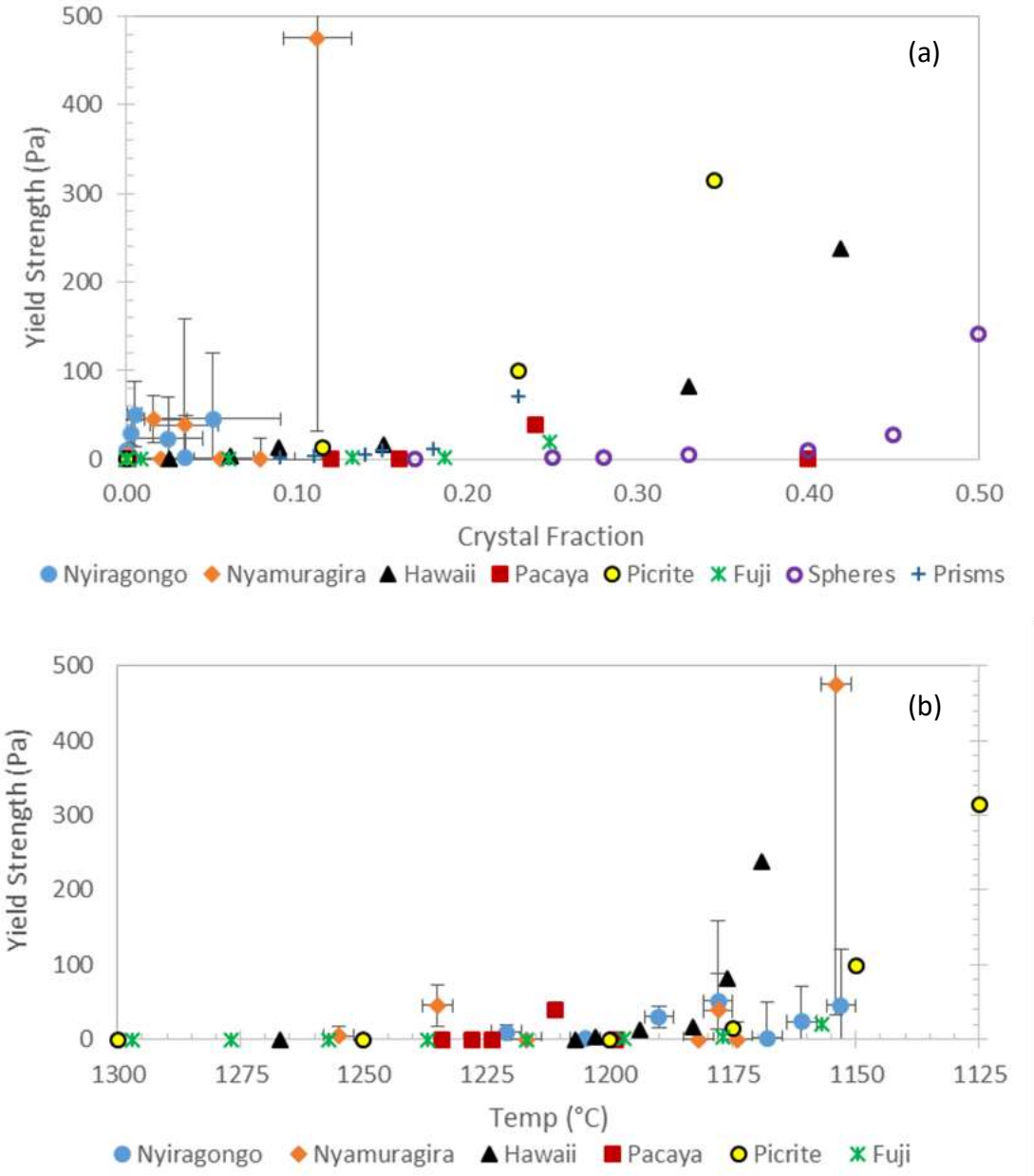

Figure 12. *Yield strength estimates versus (a) crystal fraction and (b) temperature for Nyiragongo (blue circles) and Nyamuragira (orange diamonds) plotted with estimates of other studies. The black triangles (Hawaii) are from Sehlke et al. (2014); the red squares (Pacaya) are from Soldati et al. (2015); the yellow circles (Picrite) are from Ryerson et al. (1988); the purple rings and blue crosses are spherical and prismatic particles in an analog suspense from Hoover et al. (2001).*

models usually over-estimate yield strength values for lavas and there is much better agreement between studies using power law models. This holds true for Nyiragongo and Nyamuragira lavas as well. At the low crystal fractions achieved, no detectable yield strength was observed which is in broad agreement with these other studies. Nyamuragira may begin to develop a yield strength at $\phi_c = 0.11 \pm 0.02$ (476 ± 443 Pa) but is still within error of detection limits due to the narrow range of strain rate measurable in this experiment. Flow curves show much better fit qualities using a power law at higher temperatures and lower crystal fractions. A Herschel-Bulkley model is ideal as it allows for a yield strength to exist and a power-law fit to be achieved.

Physical effects of crystals on relative viscosity of magma

By decreasing temperature in successive experiments, it is possible to determine how increasing crystal fraction affects rheological behavior, as long as the effects of changing residual melt composition are also accounted for (Getson and Whittington, 2007). Relative viscosity (η_r) is defined as:

(8) $$\eta_r = \frac{\eta_s}{\eta_l}$$

where η_s is the apparent viscosity of the suspension and η_l is the viscosity of the coexisting, interstitial liquid at that temperature. The liquid viscosity can be determined from direct measurement or by calculation. As discussed in Sehlke et al. (2014) and Sehlke et al. (2015), the direct measurement of a synthesized interstitial melt composition is a much more reliable method due to the inaccuracies of calculations using models such as Hui and Zhang (2007) or Giordano et al. (2008).

Viscosity data for both evolved compositions are listed in Tables 7a and 7b. In the case of Nyiragongo, this method of determining relative viscosity is invalid due to the lack of crystallization and limited change in melt chemistry over the first ~50°C of undercooling. Figure 13 shows the modeled viscosity of the initial bulk liquid and the evolved melt composition with measured apparent viscosity data from each subliquidus experiment. Instead of the melt evolving in a linear fashion between the bulk and evolved liquids, the apparent viscosity data follow the bulk trend until a significant amount of crystallization occurs to begin changing the melt chemistry. This can be observed in the graphs of major oxide chemistry in Figure 6. Thus, it is assumed that the effect of crystals on the relative viscosity is ultimately negligible over this temperature range. Chemical analyses of the synthesized, evolved compositions compared to the subliquidus glass compositions are compiled in Table 8. In both cases, the synthesized, evolved compositions are slightly deficient in iron. This creates a more polymerized melt which results in a slightly higher viscosity. The additional uncertainty arising from the oxidation state of the melt may partially explain why the interstitial melt viscosity is higher than the viscosity of the melt/ crystal mixture, although within experimental uncertainty.

Implications for volcanic hazards

Giordano et al. (2007) looked at similar lava samples erupted from the Munigi Fissure during the 2002 Nyiragongo eruption. They conducted dynamic cooling experiments in which they determine a liquidus temperature by the departure from the pure liquid viscosity trend (~1100°C). This method severely underestimates the liquidus temperature that we determined by calorimetry (~1220°C) and by visual confirmation of

Table 7a. *Crystal free, liquid viscosity measurements at high temperature and near the glass transition for the evolved Nyiragongo composition. Points listed in red were omitting from data fitting due to possible crystallization.*

Nyiragongo (eNYI)					core 1
Temp (°C)	10,000/T (K^{-1})	log η (Pa s)	Temp (°C)	10,000/T (K^{-1})	log η (Pa s)
1172.4	6.92	2.88	687.0	10.42	11.07
1196.6	6.80	2.72	696.5	10.31	10.61
1222.0	6.69	2.56	714.5	10.13	10.04
1248.6	6.57	2.41	719.6	10.07	9.78
1274.2	6.46	2.27	724.7	10.02	9.76
1299.2	6.36	2.12	729.6	9.97	9.50
1312.2	6.31	2.07	734.5	9.92	9.53
1323.9	6.26	2.01	739.6	9.87	9.28
1349.1	6.16	1.88	744.68	9.82	9.50
1373.3	6.07	1.78	749.60	9.78	9.15
1398.4	5.98	1.66			
1411.4	5.94	1.60			
1423.6	5.89	1.55			
1449.1	5.81	1.44	TVF parameters		
1474.5	5.72	1.33	A	-3.11	
1500.9	5.64	1.25	B	5102.24	
1511.7	5.60	1.14	C	599.80	
1525.2	5.56	1.16			
1551.0	5.48	1.07	RMSD	0.04 log Pa s	
1576.8	5.41	0.98			
1582.6	5.39	0.94			

crystals using BSE images. Figure 13 shows the apparent viscosity following the trend of the bulk liquid until significant crystallization occurs after ~50°C of undercooling. Giordano et al. (2007) may not have realized the liquidus had been crossed prior to the departure from the bulk liquid trend due to the very small crystal fraction that does not noticeably impact viscosity. They also argue for superliquidus eruption temperatures

Table 7b. *Crystal free, liquid viscosity measurements at high temperature and near the glass transition for the evolved Nyamuragira composition. Points listed in red were omitted from data fitting due to insufficient deformation in the segment (<10 μm after relaxation).*

Nyamuragira (eNYA)					core 1
Temp (°C)	10,000/T (K^{-1})	log η (Pa s)	Temp (°C)	10,000/T (K^{-1})	log η (Pa s)
1197.4	6.80	3.20	704.7	10.23	11.85
1226.2	6.67	3.01	705.8	10.22	11.95
1247.1	6.58	2.87	716.0	10.11	11.48
1274.2	6.46	2.70	723.8	10.03	10.75
1297.4	6.37	2.57	728.9	9.98	10.42
1311.7	6.31	2.48	733.7	9.93	10.63
1323.3	6.26	2.42	736.7	9.90	10.32
1345.2	6.18	2.31	743.8	9.83	10.29
1373.7	6.07	2.16	746.5	9.81	10.17
1399.7	5.98	2.03	754.0	9.74	9.99
1411.6	5.94	1.98	756.5	9.71	9.92
1424.4	5.89	1.92	764.2	9.64	9.72
1448.7	5.81	1.81	766.5	9.62	9.63
1473.8	5.72	1.70			
1499.0	5.64	1.59	TVF parameters		
1510.6	5.61	1.55	A	-2.75	
1523.5	5.57	1.48	B	4918.80	
1547.9	5.49	1.36	C	641.82	
1575.9	5.41	1.31			
1580.6	5.39	1.22	RMSD	0.05 log Pa s	

which is a key implication for this system. Should lavas be erupted at superliquidus conditions, or even near-liquidus conditions, the lava would remain fluid for much longer before crystal nucleation and growth begin increasing viscosity.

Favalli et al. (2006) modeled future lava flows from Nyiragongo into the city of Goma. However, no attempt was made to incorporate rheological properties. In this study, a flow thickness of 2-4 m was taken from field observations of lava flows

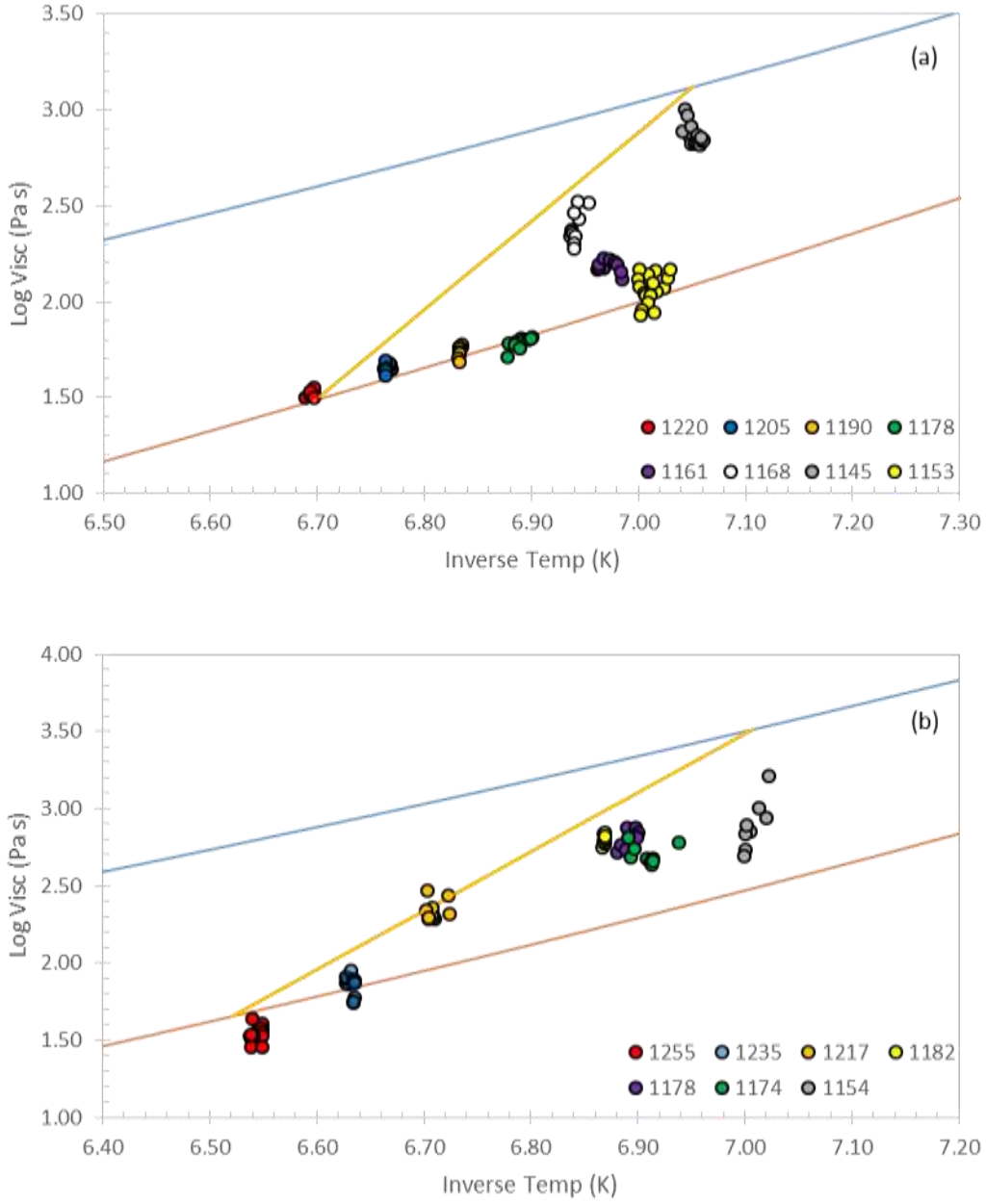

Figure 13. *Viscosity modeled for the bulk remelt (orange line) and the most evolved subliquidus melt composition (blue line). Points plotted are apparent viscosities of each successive subliquidus experiment. (a) Nyiragongo shows a non-linear crystallization path which prevents the viscosity estimation of intermediate compositions by linear interpolation. (b) Nyamuragira shows a more linear crystallization trend before deviating at the 1182°C experiment.*

Table 8. *Evolved interstitial glass compositions for Nyiragongo (eNYI) and Nyamuragira (eNYA). Compositions are listed alongside EPMA analysis for the glass composition to be synthesized. Both synthesized glasses are slightly deficient in iron which may introduce larger uncertainties on interpolated viscosities of the intermediate compositions.*

	eNYI		1143 gl		eNYA		1165 gl	
	wt%	(2σ)	wt%	(2σ)	wt%	(2σ)	wt%	(2σ)
SiO_2	41.89	0.14	41.34	0.08	48.27	0.21	48.07	0.18
TiO_2	3.00	0.03	2.90	0.04	3.41	0.04	3.42	0.05
Al_2O_3	16.37	0.06	15.30	0.06	17.97	0.11	17.25	0.12
Cr_2O_3	0.01	0.00	0.00	0.01	0.02	0.01	0.00	0.00
FeO	7.11	0.07	8.27	0.06	5.90	0.04	6.90	0.05
MnO	0.33	0.03	0.24	0.01	0.36	0.02	0.29	0.02
MgO	3.44	0.02	3.41	0.02	4.07	0.04	4.09	0.02
CaO	13.46	0.04	12.89	0.04	10.36	0.07	10.14	0.09
Na_2O	6.06	0.07	5.73	0.03	4.07	0.03	3.92	0.06
K_2O	6.03	0.04	5.68	0.04	4.34	0.03	4.25	0.05
P_2O_5	1.60	0.03	1.58	0.04	0.77	0.02	0.75	0.04
TOTAL	99.31	0.24	97.34	0.13	99.55	0.20	99.06	0.30

originating from the Munigi fissure. Flow thickness is directly proportional to yield strength parameters which can be calculated by the following equation from Hulme (1974):

(9) $$h_c = \frac{\sigma_y}{\rho g tan(\alpha)}$$

where h_c is the critical flow thickness required for flow advancement, σ_y is the yield strength, ρ is density, g is gravity, and α is the flow slope. Estimate of the effective yield strength range from the order of 10^2 Pa to 10^3 Pa depending on local slope estimates. Without the parameters of rheological behavior, like yield strength and viscosity (particularly the evolution of viscosity as stated above), an accurate depiction of lava flow paths cannot truly be realized. Other studies have attempted numerical simulations

of lava flow paths (Favalli et al., 2009; Chirico et al., 2009) which only take into account flows from the fracture system. However, parasitic cones that exist throughout the region, including downtown Goma (Tedesco et al., 2007; Chakrabarti et al., 2009a), are neglected. These possible vent locations pose as great of a threat to the people of Goma as lavas erupting from the fissures and should be considered in modeling. A truly accurate hazard model remains to exist that accounts for both the rheological evolution of the lava as well as the variation in vent location.

Volcano Morphology

Reconstructing the early building period of Nyiragongo has proven to be extremely difficult. Access to any deeper structures of the volcano are obscured due to lack of erosion coupled with the overlaying of new material from recent activity in the caldera and along the fissures (Demant et al., 1994; Chakrabarti et al., 2009a). Exposure in the caldera is only ~400 m which likely represents activity only as old as the Holocene (Demant et al., 1994). While the true evolution of erupted material will have to wait until pertinent field work can be undertaken, it can be speculated as to why such low viscosity, basaltic lavas erupt from a stratovolcano.

The compositional distinction in volcanism between Nyiragongo and Nyamuragira over such a small spatial range can be explained by melting of compositionally distinct parts of a heterogeneous mantle plume (Ebinger et al., 1989; Hofmann et al., 1997; Chakrabarti et al., 2009b). During the initial building period of the Nyiragongo stratovolcano, lavas were most likely more silicic allowing for a steeper edifice to form. Influx of more primitive material may have subsequently changed the composition of lavas to the more mafic, foiditic material observed in recent eruptions. A

similar situation has been observed at Pacaya volcano in the Central American Volcanic Arc complex. Bardintzeff and Deniel (1992) describe an initial building phase of basalts followed by andesitic to dacitic dome emplacement followed again by basaltic lavas being erupted most recently. Compositions of the source material for Nyamuragira may not have had such dynamic changes as may have occurred at Nyiragongo. Lavas may have been mafic for the entirety of the volcano's active history creating the gently sloping shield edifice that continues to be built upon with the most recent tephrite to basanite lavas.

Conclusions

Despite their broad chemical similarity, lavas from Nyiragongo and Nyamuragira have very distinct rheological behaviors during cooling and crystallization. In this instance, the stratovolcano uncharacteristically erupts lower viscosity lavas than the nearby shield volcano most likely due to a heterogeneous mantle plume source. Nyiragongo lavas have a lower liquidus temperature and begin crystallizing after a larger degree of undercooling than those of Nyamuragira. There is little crystallization that occurs over the range of experimental temperatures in either composition (NYI 1145°C, $\phi_c = 0.05 \pm 0.02$; NYA 1154°C, $\phi_c = 0.11 \pm 0.02$) suggesting that the increase in viscosity is mainly due to cooling effects rather than any physical or chemical effects of crystallization. Near-Newtonian behavior continues to be observed with the Nyiragongo lavas until ~50-60°C undercooled where pseudo-plastic behavior becomes dominant. Nyamuragira begins demonstrating this pseudo-plastic behavior at temperatures much closer to the liquidus. Most previous studies of other basaltic compositions place the start of pseudo-plastic behavior at crystal fractions around 0.05-0.10 which is in agreement with our findings for Nyiragongo and Nyamuragira. No detectable yield strength was observed in either sample at the low crystal fractions which also agrees with many other studies suggesting yield strength development occurs at much higher crystal fractions than we were able to achieve. Nyiragongo, ultimately, has proven to produce deadly lava flows. They are particularly dangerous because of how fluid the lavas remain after eruption due to the lack of crystallization. Viscosity increase and yield strength development remain relatively unchanged over the range of undercooling before crystallization occurs. The lava crystallizes rapidly once this temperature threshold is

reached, so much so that experiments at these temperatures are beyond the limitations of the instrumentation available. This rheological threshold that occurs between 1160°C and 1140°C means lava flow movement will quickly be inhibited shortly after reaching this temperature range. Thus far, hazard modeling has been insufficient to provide an all-encompassing picture of the dangers posed by Nyiragongo to the city of Goma. There are few places in the world where a volcano poses such an imminent threat to a highly populated, urban area. With the influx of more people and refugees from the political instability of surrounding areas, the potential exists for a humanitarian crisis of even greater magnitude than that of the 2002 eruption. Continued work must be done to adequately prepare for and mitigate hazards facing the over 500,000 residents of Goma.

References

Acocella, V., and M. Neri (2009) Dike propagation in volcanic edifices: Overview and possible developments, *Tectonophysics*, *471*, 67–77, doi:10.1016/j.tecto.2008.10.002.

Andersen, T., M. Elburg, M. Erambert (2012) Petrology of combeite- and götzenite-bearing nephelinite at Nyiragongo, Virunga Volcanic Province in the East African Rift. *Lithos, 152,* pp. 105–12.

Aoki, K., T. Yoshida, K. Yusa, Y. Nakamura (1985) Petrology and geochemistry of the Nyamuragira Volcano, Zaire. *J Volcanol Geotherm Res 25*:1–28.

Armstrong, J.T. (1995) CITZAF: a package of correction programs for the quantitative electron microbeam X-ray analysis of thick polished materials, thin films, and particles. *Microbeam Anal 4*:177–200.

Bardintzeff, J. M., and C. Deniel (1992) Magmatic evolution of Pacaya and Cerro Chiquito volcanological complex, Guatemala. *Bull. Volcanol. 54*(4), 267-283.

Bluth, G.J.S., and S.A. Carn (2008) Exceptional sulfur degassing from Nyamuragira volcano, 1979–2005, *Int. J. Rem. Sens.*, *29*(22), 6667–6685, doi:10.1080/01431160802168434.

Burt, M.L., G. Wadge, and W.A. Scott (1994) Simple Stochastic modeling of the eruption history of a basaltic volcano: Nyamuragira, Zaire, *Bull. Volcanol.*, *56*(2), 87–97.

Calais E, C.J. Ebinger, C. Hartnady, and J.M. Nocquet (2006) Kinematics of the East African Rift from GPS and earthquake slip vector data, in The Afar Volcanic Province Within the East African Rift System, vol. *259*, edited by G. Yirgu, C.J.

Ebinger, and P.K.H. Maguire, pp. 9–22, *Geol. Soc. Spec. Publ.*, London, U. K

Campion, R. (2014) New lava lake at Nyamuragira volcano revealed by combined ASTER and OMI SO_2 measurements, *Geophys. Res. Lett.*, *41*, 7485–7492, doi:10.1002/2014GL061808.

Carn, S.A., and G.J.S. Bluth (2003) Prodigious sulfur dioxide emissions from Nyamuragira volcano, D.R. Congo, *Geophys. Res. Lett.*, *30*(23), 2211, doi:10.1029/2003GL018465.

Carn, S.A. (2002) Eruptive and passive degassing of sulphur dioxide at Nyiragongo volcano (D. R. Congo): the 17 January 2002 eruption and its aftermath. *Acta Vulcanologica* vol. *4*(1-2).

Chakrabarti, R., A.R. Basu, A.P. Santo, D. Tedesco, O. Vaselli (2009a) Isotopic and geochemical study of the Nyiragongo and Nyamuragira volcanics in the western rift of the East African Rift System. *Chem. Geol*. *259*:273–289.

Chakrabarti, R., K.W.W. Sims, A.R. Basu, M. Reagan, J. Durieux (2009b) Timescales of magmatic processes and eruption ages of the Nyiragongo volcanics from 238U-230Th-226Ra-210Pb disequilibria. *Earth Planet Sci. Lett*. *288*:149–157.

Chirico, G.D., M. Favalli, P. Papale, E. Boschi, M.T. Pareschi, A. Mamou-Mani (2009) Lava flow hazard at Nyiragongo volcano, DRC. 2. Hazard reduction in urban areas. *Bull. Volcanol*. *71*(4), 375–387.

Coppola, D., and C. Cigolini (2013) Thermal regimes and effusive trends at Nyamuragira volcano (DRC) from MODIS infrared data, *Bull. Volcanol. 75*(8), 744, doi:10.1007/s00445-013-0744-z.

Dawson, J.B., H. Pinkerton, G.E. Norton, D.M. Pyle (1990) Physicochemical properties

of alkali carbonatite lavas: data from the 1988 eruption of Oldoinyo Lengai. *Geology 18*:260–263.

Demant, A., P. Lestrade, R.T. Lubala, A.B. Kampunzu and J. Durieux (1994) Volcanological and petrological evolution of Nyiragongo volcano, Virunga volcanic field, Zaire. *Bull. Volcanol*. *56*, 47-61.

Dingwell, D.B., D. Virgo (1988) Melt viscosities in the Na2O–FeO–Fe2O3–SiO2 system and factors controlling the relative viscosities of fully polymerized silicate melts. *Geochim Cosmochim Acta 52*:395–403

Ebinger, C., T. Bechtel, D. Forsyth, C. Bowin, (1989) Effective elastic plate thickness beneath the east African and Afar plateaus and dynamic compensation for the uplifts. *J. Geophys. Res. 94*, 2883–2901.

Favalli, M., G.D. Chirico, P. Papale, M.T. Pareschi, M. Coltelli, N. Lucana, and E. Boschi (2006) Computer simulations of lava flow paths in the town of Goma, Nyiragongo volcano, Democratic Republic of Congo, *J. Geophys. Res*. *111*, B06202, doi:10.1029/2004JB003527.

Gent, A.N. (1960) Theory of the parallel plate viscometer. *British Journal of Applied Physics*, *11*(2), 85.

Getson, J.M., A.G. Whittington (2007) Liquid and magma viscosity in the anorthite-forsterite-diopside-quartz system and implications for the viscosity-temperature paths of cooling magmas. *J. Geophys. Res*. *112*(B10)

Ghiorso, M.S. and R.O. Sack (1995) Chemical Mass Transfer in Magmatic Processes. IV. A Revised and Internally Consistent Thermodynamic Model for the Interpolation and Extrapolation of Liquid-Solid Equilibria in Magmatic Systems at Elevated

Temperatures and Pressures. *Contributions to Mineralogy and Petrology*, *119*, 197-212.

Giordano, D., D.B. Dingwell (2003) Non-Arrhenian multicomponent melt viscosity: a model. *Earth Planet. Sci. Lett*., *208*, pp. 337–349

Giordano, D., M. Polacci, A. Longo, P. Papale, D.B. Dingwell, E. Boschi, M. Kasereka (2007) Thermo-rheological magma control on the impact of highly fluid lava flows at Mt. Nyiragongo. *Geophys. Res. Lett*., *34* doi: 10.1029/2006GL028459.

Giordano, D., J.K. Russell, and D.B. Dingwell (2008) Viscosity of magmatic liquids: A model, *Earth Planet. Sci. Lett*., *271*(1–4), 123–134.

Gualda, G.A.R., M.S. Ghiorso, R.V. Lemons, T.L. Carley (2012) Rhyolite-MELTS: A modified calibration of MELTS optimized for silica-rich, fluid-bearing magmatic systems. *Journal of Petrology*, *53*, 875-890.

Head, E.M., A.M. Shaw, P.J. Wallace, K.W.W. Sims, and S.A. Carn (2011) Insight into volatile behavior at Nyamuragira volcano (D.R. Congo, Africa) through olivine-hosted melt inclusions, *Geochem. Geophys. Geosyst. 12*, Q0AB11, doi:10.1029/2011GC003699.

Hofmann, C., V. Courtillot, G. Feraud, P. Rochette, G. Yirgu, E. Ketefo, and R. Pik, (1997) Timing of the Ethiopian flood basalt event and implications for plume birth and global change. *Nature*, *389*(6653), 838-841.

Hoover, S.R., K.V. Chasman, M. Manga, (2001) The yield strength of subliquidus basalts—experimental results. *J. Volcanol. Geotherm. Res. 107*:1–18.

Hui, H., and Y. Zhang (2007) Towards a general viscosity equation for natural anhydrous and hydrous silicate melts, *Geochim. Cosmochim. Acta*, *71*, 403–416.

Hulme, G. (1974) The interpretation of lava flow morphology. *Geophys. J. Int.* *39*(2):361–383. doi:10.1111/j.1365-246X.1974.tb05460.

Ishibashi, H. (2009) Non-Newtonian behavior of plagioclase-bearing basaltic magma: Subliquidus viscosity measurement of the 1707 basalt of Fuji volcano, Japan. *J. Volcanol. Geotherm. Res. 181*(1), 78-88.

Ishibashi, H., and H. Sato, (2007) Viscosity measurements of subliquidus magmas: Alkali olivine basalt from the Higashi-Matsuura district, Southwest Japan. *J. Volcanol. Geotherm. Res*. *160*(3), 223-238.

Ishibashi, H., and H. Sato (2010) Bingham fluid behavior of plagioclase-bearing basaltic magma: Reanalyses of laboratory viscosity measurements for Fuji 1707 basalt. *Journal of Mineralogical and Petrological Sciences*, *105*(6), 334-339.

Kerr, R.C., and J.R. Lister (1991) The effects of shape on crystal settling and on the rheology of magmas, *J. Geol*. *99*(3), 457–467.

Kress, V.C., and I.S. Carmichael, (1991) The compressibility of silicate liquids containing Fe2O3 and the effect of composition, temperature, oxygen fugacity and pressure on their redox states. *Contributions to Mineralogy and Petrology*, *108*(1-2), 82-92.

Mysen, B. and P. Richet (2005) Silicate Glasses and Melt, Chapter 10: iron-bearing Melts, *Elsevier Science*, Amsterdam, Netherlands.

Platz, T., S.F. Foley, L. Andrè (2004) Low-pressure fractionation of the Nyiragongo volcanic rocks, Virunga Province, D.R. Congo. *J. Volcanol. Geotherm. Res*. *136*, pp. 269–295.

Pouclet, A. (1976) Volcanologie du rift de l'Afrique Centrale. Le Nyamulagira dans les

Virunga: essai de magmatologie du rift (PhD Thesis) Université de Paris-Sud, Centre d'Orsay, France (597 pp.)

Rasband, W.S., ImageJ, U. S. National Institutes of Health, Bethesda, Maryland, USA, http://imagej.nih.gov/ij/, 1997-2015.

Ryerson, F.J., H.C. Weed, and A.J. Piwinskii (1988) Rheology of subliquidus magmas: 1. Picritic compositions, *J. Geophys. Res*. *93,* 3421–3436, doi:10.1029/JB093iB04p03421.

Saria, E., E. Calais, D.S. Stamps, D. Delvaux, and C.J.H. Hartnady (2014) Present-day kinematics of the East African Rift, *J. Geophys. Res: Solid Earth*, *119,* 3584–3600, doi:10.1002/2013JB010901.

Sawyer, G.M., S.A. Carn, V.I. Tsanev, C. Oppenheimer, and M. Burton (2008) Investigation into magma degassing at Nyiragongo volcano, Democratic Republic of the Congo. *Geochem. Geophys. Geosyst. 9* (2).

Schilling, J.G., R.H. Kingsley, B.B. Hanan, B.L. McCully (1992) Nd–Sr–Pb isotopic variations along the Gulf of Aden: evidence for Afar mantle plume-continental lithosphere interaction *J. Geophys. Res*. *97,* pp. 10927–10966.

Schuessler, J.A., R.E. Botcharnikov, H. Behrens, V. Misiti, C. Freda, (2008) Amorphous materials: properties, structure, and durability: oxidation state of iron in hydrous phono-tephritic melts. *Am. Mineral*. *93*(10):1493–1504.

Sehlke, A., A. Whittington, B. Robert, A. Harris, L. Gurioli, & E. Médard (2014) Pahoehoe to aa transition of Hawaiian lavas: an experimental study. *Bull. Volcanol. 76*(11), 1-20.

Sehlke, A., & A. Whittington (2015) Rheology of lava flows on Mercury: An analog

experimental study. *J. Geophys. Res: Planets*, *120*(11), 1924-1955.

Sharma, K., S. Blake, S. Self, A.J. Krueger, (2004) SO2 emissions from basaltic eruptions, and the excess sulfur issue. *Geophys. Res. Lett. 31* (L13612). doi:10.1029/2004GL019688.

Shinohara, H. (2008) Excess degassing from volcanoes and its role on eruptive and intrusive activity. *Rev. Geophys*. *46* (RG4005). doi:10.1029/2007RG000244.

Simkin, T., L. Siebert (1994) Volcanoes of the World. Geoscience Press, Tucson, Arizona pp.v349.

Smets, B., N. d'Oreye, F. Kervyn, M. Kervyn, F. Albino, S.R. Arellano, ... and J. Fernández, (2014) Detailed multidisciplinary monitoring reveals pre-and co-eruptive signals at Nyamulagira volcano (North Kivu, Democratic Republic of Congo). *Bull. Volcanol. 76*(1), 1-35.

Smets, B., M. Kervyn, N. d'Oreye, and F. Kervyn, (2015) Spatio-temporal dynamics of eruptions in a youthful extensional setting: Insights from Nyamulagira Volcano (DR Congo), in the western branch of the East African Rift. *Earth-Science Reviews*.

Soldati, A., A. Bollasina, G. Chigna, A. Sehlke, and A.G. Whittington, (2015) Field and experimental constraints on the rheology of arc basaltic lavas: the January 2014 Eruption of Pacaya (Guatemala). *Bull. Volcanol.* (in press).

Stein, D.J., F.J. Spera, (1998) New high-temperature rotational rheometer for silicate melts, magmatic suspensions, and emulsions. *Rev Sci Instrum 69*:3398–3402. doi:10.1063/1.1149106.

Tazieff, H. (1977) An exceptional eruption: Mt. Nyiragongo, January 10th, 1977. *Bull.*

Volcanol. 40(3), 189-200.

Tazieff, H. (1984) Mt. Nyiragongo: renewed activity of the lava lake. *J. Volcanol. Geotherm. Res. 20*, 267-280.

Tedesco, D., O. Vaselli, P. Papale, S.A. Carn, M. Voltaggio, G.M. Sawyer, J. Durieux, M. Kasereka, and F. Tassi (2007) January 2002 volcano-tectonic eruption of Nyiragongo volcano, Democratic Republic of Congo, *J. Geophys. Res*. *112,* B09202, doi:10.1029/2006JB004762.

Vogel, D.H. (1921) Temperaturabhängigkeitsgesetz der Viskosität von Flüssigkeiten. Phys Z XXII:645–646.

Von Götzen, A. (1896) Durch Afrika von Ost nach West. Dietrich Reimer, Berlin.

Wadge, G., and L. Burt (2011), Stress field control of eruption dynamics at a rift volcano: Nyamuragira, D.R. Congo, *J. Volcanol. Geotherm. Res. 207*(1–2), 1–15, doi:10.1016/j.jvolgeores.2011.06.012.

Wallace, P.J. (2001) Volcanic SO2 emissions and the abundance and distribution of exsolved gas in magma bodies. *J Volcanol. Geotherm. Res*. *108*:85–106.

Wafula, M.D., N. Zana, M. Kasereka, and H. Hamaguchi (n.d.) The Nyiragongo Volcano: A Case Study for the Mitigation of Hazards on an African Rift Volcano, Virunga Region, Western Rift Valley.

Wauthier, C., V. Cayol, M. Poland, F. Kervyn, N. d'Oreye, A. Hooper, S. Samsonov, K. Tiampo, and B. Smets (2013) Nyamulagira's plumbing system inferred from 15 years of InSAR, *Geol. Soc. London Spec. Publ., 380,* doi:10.1144/SP380.9.

Webb, S.L., and Dingwell, D.B. (1990) The onset of non-Newtonian rheology of silicate melts. *Physics and Chemistry of Minerals*, *17*(2), 125-132.

Whittington, A.G., B.M. Hellwig, H. Behrens, B. Joachim, A. Stechern, F. Vetere, (2009) The viscosity of hydrous dacitic liquids: Implications for the rheology of evolving silicic magmas. *Bull. Volcanol*. *71*:185–199. doi:10.1007/s00445-008-0217-y.

Wilson, A.D. (1960) The micro-determination of ferrous iron in silicate minerals by a volumetric and a colorimetric method. *Analyst 85*(1016):823–827.